WRDC-TR-89-213

AD-A221 942

A HEAT TRANSFER ANALYSIS FOR ROUGH TURBINE AIRFOILS

Lit S. Han and Majid Delpassand
Department of Mechanical Engineering
The Ohio State University
Columbus, Ohio 43210

January 16, 1990

Final Report for Period April 1986-March 1989

AERO PROPULSION AND POWER LABORATORY
WRIGHT RESEARCH DEVELOPMENT CENTER
AIR FORCE SYSTEMS COMMAND
WRIGHT-PATTERSON AIR FORCE BASE, OHIO 45433-6563

NOTICE

WHEN GOVERNMENT DRAWINGS, SPECIFICATIONS, OR OTHER DATA ARE USED FOR ANY PURPOSE OTHER THAN IN CONNECTION WITH A DEFINITELY GOVERNMENT-RELATED PROCUREMENT, THE UNITED STATES GOVERNMENT INCURS NO RESPONSIBILITY OR ANY OBLIGATION WHATSOEVER. THE FACT THAT THE GOVERNMENT MAY HAVE FORMULATED OR IN ANY WAY SUPPLIED THE SAID DRAWINGS, SPECIFICATIONS, OR OTHER DATA, IS NOT TO BE REGARDED BY IMPLICATION, OR OTHERWISE IN ANY MANNER CONSTRUED, AS LICENSING THE HOLDER, OR ANY OTHER PERSON OR CORPORATION; OR AS CONVEYING ANY RIGHTS OR PERMISSION TO MANUFACTURE, USE, OR SELL ANY PATENTED INVENTION THAT MAY IN ANY WAY BE RELATED THERETO.

THIS REPORT HAS BEEN REVIEWED BY THE OFFICE OF PUBLIC AFFAIRS (ASD/PA) AND IS RELEASABLE TO THE NATIONAL TECHNICAL INFORMATION SERVICE (NTIS). AT NTIS IT WILL BE AVAILABLE TO THE GENERAL PUBLIC INCLUDING FOREIGN NATIONS.

THIS TECHNICAL REPORT HAS BEEN REVIEWED AND IS APPROVED FOR PUBLICATION.

Charles D MacArthur

CHARLES D. MacARTHUR, PROJ ENGR
Components Branch
Turbine Engine Division
Aero Propulsion and Power
Laboratory

Geoffrey W. Jumper

GEOFFREY W. JUMPER, Maj, USAF
Chief, Components Branch
Turbine Engine Division
Aero Propulsion and Power
Laboratory

James S Petty

JAMES S. PETTY
Acting Deputy for Technology
Turbine Engine Division
Aero Propulsion and Power

IF YOUR ADDRESS HAS CHANGED, IF YOU WISH TO BE REMOVED FROM OUR MAILING LIST, OR IF THE ADDRESSEE IS NO LONGER EMPLOYED BY YOUR ORGANIZATION PLEASE NOTIFY WRDC/POTC , WRIGHT-PATTERSON AFB, OH 45433- 6563 TO HELP MAINTAIN A CURRENT MAILING LIST.

COPIES OF THIS REPORT SHOULD NOT BE RETURNED UNLESS RETURN IS REQUIRED BY SECURITY CONSIDERATIONS, CONTRACTUAL OBLIGATIONS, OR NOTICE ON A SPECIFIC DOCUMENT.

UNCLASSIFIED
SECURITY CLASSIFICATION OF THIS PAGE

REPORT DOCUMENTATION PAGE

Form Approved
OMB No. 0704-0188

1a. REPORT SECURITY CLASSIFICATION Unclassified	1b. RESTRICTIVE MARKINGS
2a. SECURITY CLASSIFICATION AUTHORITY	3. DISTRIBUTION / AVAILABILITY OF REPORT Approved for public release; distribution unlimited.
2b. DECLASSIFICATION / DOWNGRADING SCHEDULE	
4. PERFORMING ORGANIZATION REPORT NUMBER(S) RF Project 765354/718268	5. MONITORING ORGANIZATION REPORT NUMBER(S) WRDC-TR-89-2135
6a. NAME OF PERFORMING ORGANIZATION The Ohio State University Research Foundation 6b. OFFICE SYMBOL (If applicable) (OSURF)	7a. NAME OF MONITORING ORGANIZATION Aero Propulsion and Power Laboratory (WRDC/ Wright Research Development Center POTC)
6c. ADDRESS (City, State, and ZIP Code) 1314 Kinnear Road Columbus, Ohio 43212	7b. ADDRESS (City, State, and ZIP Code) Wright-Patterson Air Force Base, Ohio 45433-6563
8a. NAME OF FUNDING / SPONSORING ORGANIZATION Aero Propulsion and Power Laboratory 8b. OFFICE SYMBOL (If applicable) WRDC/POTC	9. PROCUREMENT INSTRUMENT IDENTIFICATION NUMBER F33615-86-K-2621
8c. ADDRESS (City, State, and ZIP Code) Wright-Patterson Air Force Base, Ohio 45433-6563	10. SOURCE OF FUNDING NUMBERS PROGRAM ELEMENT NO. 62203F; PROJECT NO. 3066; TASK NO 14; WORK UNIT ACCESSION NO. 15

11 TITLE (Include Security Classification)
A Heat Transfer Analysis for Rough Turbine Airfoils

12 PERSONAL AUTHOR(S)
Dr. Lit S. Han and Majid Delpassand, Department of Mechanical Engineering, Ohio State Univ.

13a. TYPE OF REPORT	13b. TIME COVERED	14. DATE OF REPORT (Year, Month, Day)	15. PAGE COUNT
Final	FROM 4/86 TO 3/89	1990, January, 16	85

16 SUPPLEMENTARY NOTATION

17 COSATI CODES			18. SUBJECT TERMS (Continue on reverse if necessary and identify by block number)
FIELD	GROUP	SUB-GROUP	Turbine blades, vanes, surface roughness, turbulent boundary layer, heat transfer, ~~and~~ augmentation.

19 ABSTRACT (Continue on reverse if necessary and identify by block number)

In this research program, a methodology has been developed to calculate the increased heat transfer to turbine airfoils with surface roughness. The new model is adaptable to methods of finite-difference calculation, as opposed to correlation relations currently in use. The model utilizes an amplification factor for the thermal mixing length which is dependent on the local roughness height and surface shear stress.

20 DISTRIBUTION / AVAILABILITY OF ABSTRACT ☒ UNCLASSIFIED/UNLIMITED ☐ SAME AS RPT ☐ DTIC USERS	21 ABSTRACT SECURITY CLASSIFICATION Unclassified
22a NAME OF RESPONSIBLE INDIVIDUAL Charles D. MacArthur	22b. TELEPHONE (Include Area Code) (513) 255-4830 22c. OFFICE SYMBOL WRDC/POTC

DD Form 1473, JUN 86 *Previous editions are obsolete.*

SECURITY CLASSIFICATION OF THIS PAGE
UNCLASSIFIED

FOREWORD

The research reported here was initiated to analyze, by finite difference schemes, the effects of surface roughness on friction and heat transfer. Such need becomes particularly acute in gas turbine applications where the gas streams are at very high temperatures and may carry particulate matters. For turbine components exposed to this type of environment, the surface finish quickly becomes eroded, resulting in a roughened appearance. Past experience indicates that rough surface compressor blades produce reduced performance, and rough turbine airfoils are susceptible to damage by higher heat transfer, necessitating more cooling requirements.

In previous research sponsored by the Aero Propulsion Laboratory, AFWAL, a basic formulation of analyzing the roughness effects on friction was completed. In this continuing effort, the frictional aspect is extended to include the effect of density of the roughness elements. More significantly, analysis was undertaken to address the heat transfer effect, with a particular emphasis on gas flows (Pr=0.7).

Support for the research program was provided by the Turbine Engine Division, Aero Propulsion Laboratory, U.S. Air Force, with Charles D. MacArthur monitoring. His assistance during the course of investigation is appreciated.

TABLE OF CONTENTS

LIST OF ILLUSTRATIONS

NOMENCLATURE

A_p	=	Projected area of roughness in the flow direction, Eq (9)
A_s	=	Windward surface area of roughness, Eq (19)
B_h	=	Intercept constant in thermal wall-law, Eq (37)
B_{th}	=	Intercept constant in modified thermal wall-law, Eq (39)
B_m	=	Intercept constant in momentum wall-law, Eq (43)
c	=	specific heat at constant pressure
C_f	=	Friction Coefficient, $(2\tau/\rho U^2)$
C_m	=	Intercept constant, Eq (38)
C_h	=	Intercept constant, Eq (37)
C_{th}	=	Intercept constant, Eq (39)
d	=	Pipe diameter
D	=	Inverse of square of number of roughness elements per unit area, Eq (9)
E_m	=	Coefficient of momentum mixing length, Eq (5)
E_h	=	Coefficient of thermal mixing length, Eq (34)
F	=	Intermittancy factor, Eq (30)
G	=	Intercept constant, Eqs (4), (4a)
g	=	Dippery and Sabersky's function, Eq (22)
H	=	Shape factor (θ/δ_1)
h	=	Heat transfer coefficient
k	=	Roughness height, or molecular thermal conductivity
k^+	=	Roughness Reynolds number (ku_t/ν)
k_t	=	Turbulent thermal conductivity
K_m	=	von Karman's constant, momentum wall-law, Eq (38)
K_h	=	von Karman's constant, thermal wall-law, Eq (37)
ℓ_m	=	Momentum mixing length

ℓ_h = Thermal mixing length

ℓ^+_m = Dimensionless momentum mixing length, ($\ell_m u_t/\nu$)

ℓ^+_h = Dimensionless thermal mixing length, ($\ell_h u_t/\nu$)

L = Plate length; or roughness element spacing, Fig 1

N = Na and Habib's function, Eq (24)

Nu_d, Nu = Nusselt Number (hd/k) or (hx/k)

Pr_t = Turbulent Prandtl number, ($\varepsilon_m/\varepsilon_h$)

Pr = Fluid Prandtl number ($c\mu/k$)

q = Wall heat flux

R_m = Momentum mixing length amplification factor, Eq (5)

R_h = Thermal mixing length amplification factor, Eq (34)

Re_x = Local Reynolds number (xU/ν)

Re_k = Laboratory roughness parameter (kU/ν)

Re_d = Pipe Reynolds number (dU/ν)

Re_1 = Displacement Reynolds Number ($\delta,U/\nu$)

St = Stanton Number, $h/(\rho cU)$

S = Roughness element width, Fig. 1

T = Temperature

T^+ = Dimensionless temperature, Eq (33) $Tq/(\rho cU)$

Tu = Turbulence intensity, percent

Tu_e = Freestream turbulence intensity, percent

u = Velocity component in the x-direction

u' = Turbulent velocity in the x-direction

u_t = Friction velocity, $\sqrt{(\tau/\rho)}$

u^+	=	Dimensionless velocity (u/u_t)
U	=	Freestream velocity
v	=	Velocity component in the y-direction
v'	=	Turbulent velocity in the y-direction
W	=	Function, defined in Eq (53)
x	=	Streamwise distance from leading edge or trailing edge
y	=	Normal to surface
y^+	=	Dimensionless normal distance, yu_t/ν

GREEK SYMBOLS

β_m, β_h = slope of R_m and R_h vs. k^+, Eqs (7) and (59)

δ = Boundary layer thickness where u=0.99 of U

δ_1 = Displacement thickness

Δu^+ = Rough-surface velocity shift from wall-law

ΔT^+ = Rough-surface temperature shift from wall-law

δT^+ = Temperature difference across roughness elements, Eq (50)

ε^+_m = Turbulent viscosity ratio (μ_t/μ)

ε^+_h = Eddy conductivity ratio ($k_t/c\mu$)

θ = Momentum thickness

θ_o = Momentum thickness on smooth surface

λ_h = Roughness density function, Fig. 1

λ_r = Roughness density correlation function, Eq (9)

μ = Dynamic viscosity

μ_t = Turbulent viscosity

ν = Kinematic Viscosity (μ/ρ)

ρ = Density

τ = Shear stress

ϕ = Function, Eq (55)

SUBSCRIPTS

h Refers to thermal

m Refers to momentum

max	Refers to maximum
0	Refers to smooth surface or centerline of wake (y=0)
r	Refers to roughness
s	Refers to Nikuradse' sandgrain
t	Refers to turbulence
w	Refers to wall value

I. INTRODUCTION

The condition of a solid surface as manufactured or as a result of its service life usually exhibits surface asperities varying in magnitude and texture from one surface to another. A change in the surface appearance may be caused by erosion when turbomachines are operating with high-temperature gas streams containing impurities, dust, or unburnt fuel residues. As service time progresses, the surface finish deteriorates and the roughness increases. For the high-temperature part of gas turbines, the process is self-cascading, as increased roughness increases heat transfer which causes increased rates of heat transfer and so on.

From a basic fluid dynamic viewpoint, [24] the critical Reynolds number of transition to turbulent flow is controlled by the roughness size. It is not surprising then that more recent ablation tests indicated higher recession rates on rough surfaces. In fluid-handling machinery such as compressors, roughening of the surfaces by corrosion and erosion is known to have caused losses in their performance. Bammert and Woelk [1] examined the influence of surface quality on the efficiency, flow rate, and pressure ratio of an axial compressor. In their measurements, data were taken to determine the effects of increasing roughness on the pressure distribution around a blade profile, the development of the boundary layers, and the velocity distributions. Their results indicated an increase in the boundary layer thickness with subsequent flow separation and the disruption of pressure recovery. This phenomenon caused a substantial drop in the compressor flow rates and the achievable pressure ratios. Another instance of significant relevancy is the effect of surface roughness on the wake flow characteristics, which have a first-tier effect on the heat transfer taking place at the stagnation region of the downstream moving turbine blades. The structure of flow wakes is a direct consequence of the surface roughness on, say, the flow nozzle walls. For smooth surfaces, the wake features have been studied experimentally by Chevray and Kovasznay [4]. They showed that in the wake region, the location of maximum turbulence intensity moves away from the center line of symmetry as the main flow proceeds downstream. The introduction of surface roughnesses would no doubt alter the rate of velocity recovery in the wake, among other factors.

The present investigation addresses two related aspects: the flow and heat transfer effects. The first is an extension of the work in a previous program supported by the Aero Propulsion Laboratory and is directed to the effect of the roughness density and other flow factors. The second aspect deals with heat transfer modeling from the viewpoint of the eddy conductivity, as contrasted from viewpoints of correlation of available heat transfer measurements with roughness sizes. The objective is to be able to implement a fundamental model applicable to a variety of heating conditions. This research constitutes a second phase of investigation into the role of the surface roughness in affecting the analysis of flow resistance and augmented heat transfer. These effects become greatly magnified as the flight speed increases.

II. SURFACE ROUGHNESS EFFECTS ON BOUNDARY LAYER FLOWS

II.1 Correlation of Roughness Density: Asymptotic Case

An important parameter in describing surface roughnesses is the pattern or type of the roughness elements and their surface density of distribution. If the individual roughness protrusions are spaced widely apart, the aggregate effect on the boundary layer is small and vanishes as the space ratio becomes large compared to the roughness height. At the other extreme, if the elements are closely situated, the vortex flow developed in the inter-element cavity is reduced in intensity, again resulting in a diminished influence on the wall flow. The spatial density has long been recognized in the experimental fluid mechanics community, and it was due primarily to the work of Dvorak [9] that a more rational approach was developed. His consideration was based on the spatial density, sketched in Figure 1, with the density ratio λ_h defined as the pitch-over-width ratio. This definition is essentially a two-dimensional one. His results of correlation of a large number of surface roughnesses are focused on the roughness effects in the fully rough regime.

Starting from the equation that describes the law of the wall,

$$u^+ = 5.6\ \mathrm{Log}_{10}\ y^+ + 5.5 - \Delta u^+, \tag{1}$$

the effect of surface roughness is to have a lower intercept in Eq. (1) expressed by Δu^+, which is in turn governed by a surface roughness Reynolds number $k^+ = (k u_t/\nu)$. For large values of k^+, the fully rough regime, the relation between k^+ and Δu^+ is a logarithmic expression, as has been deduced theoretically and verified experimentally. For example, the asymptotic downshift for Nikuradse's sandgrain roughness is given by

$$\Delta u^+ = 5.6\ \mathrm{Log}_{10}\ k^+ - 2.9, \tag{2}$$

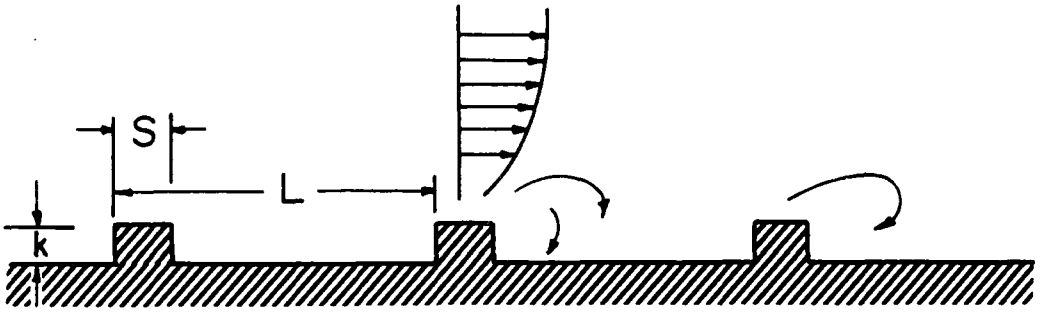

(a) Widely-Spaced Roughness Elements, $\lambda_h = L/S >> 1$.

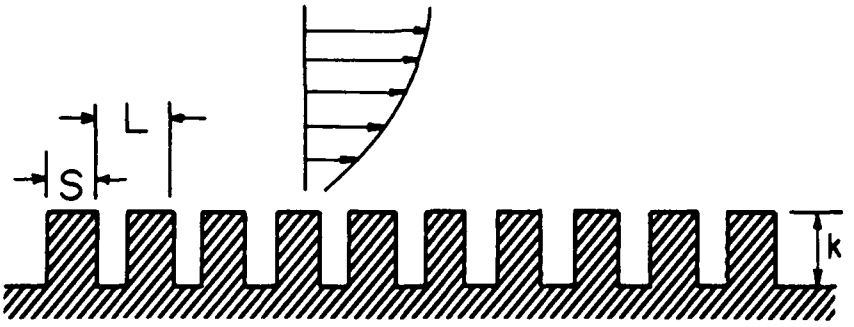

(b) Closely-Spaced Roughness Elements, $\lambda_h = L/S \sim 1$.

Figure 1. Schematics of Roughness Distribution

and for roughnesses formed by wirescreens measured by Hama [11], the equation becomes

$$\Delta u^+ = 5.6 \, \mathrm{Log}_{10} \, k^+ - 1.3. \tag{3}$$

Dvorak in his overall presentation cast Eqs. (2) and (3) into a generic expression,

$$\Delta u^+ = 5.6 \, \mathrm{Log}_{10} \, k^+ + G, \tag{4}$$

or,

$$\Delta u^+ = (1/K_m) \, \mathrm{Log}_e \, k^+ + G, \tag{4a}$$

and considered that G is a function of spatial density λ_h. His correlation is shown in Figure 2, which indicates a maximum value for G at $\lambda_h = 4.86$.

Considering his analysis in light of the exponential mixing length formulation developed in [12], the relation between Δu^+ and the momentum amplification, R_m, is reviewed here for clarity. The previously mentioned program has demonstrated that a mixing length of the exponential type can accommodate the surface roughness by an amplification (momentum) factor, R_m,

$$\ell_m^+ = R_m \, (K_m/E_m)[\exp \, (K_m u^+) - \exp \, (-K_m u^+)], \tag{5}$$

and that the law of the wall with a velocity downshift Δu^+ is recovered, with a relationship between Δu^+ and R_m given by

$$\Delta u^+ = (1/K_m) \, \mathrm{Log}_e \, (R_m). \tag{6}$$

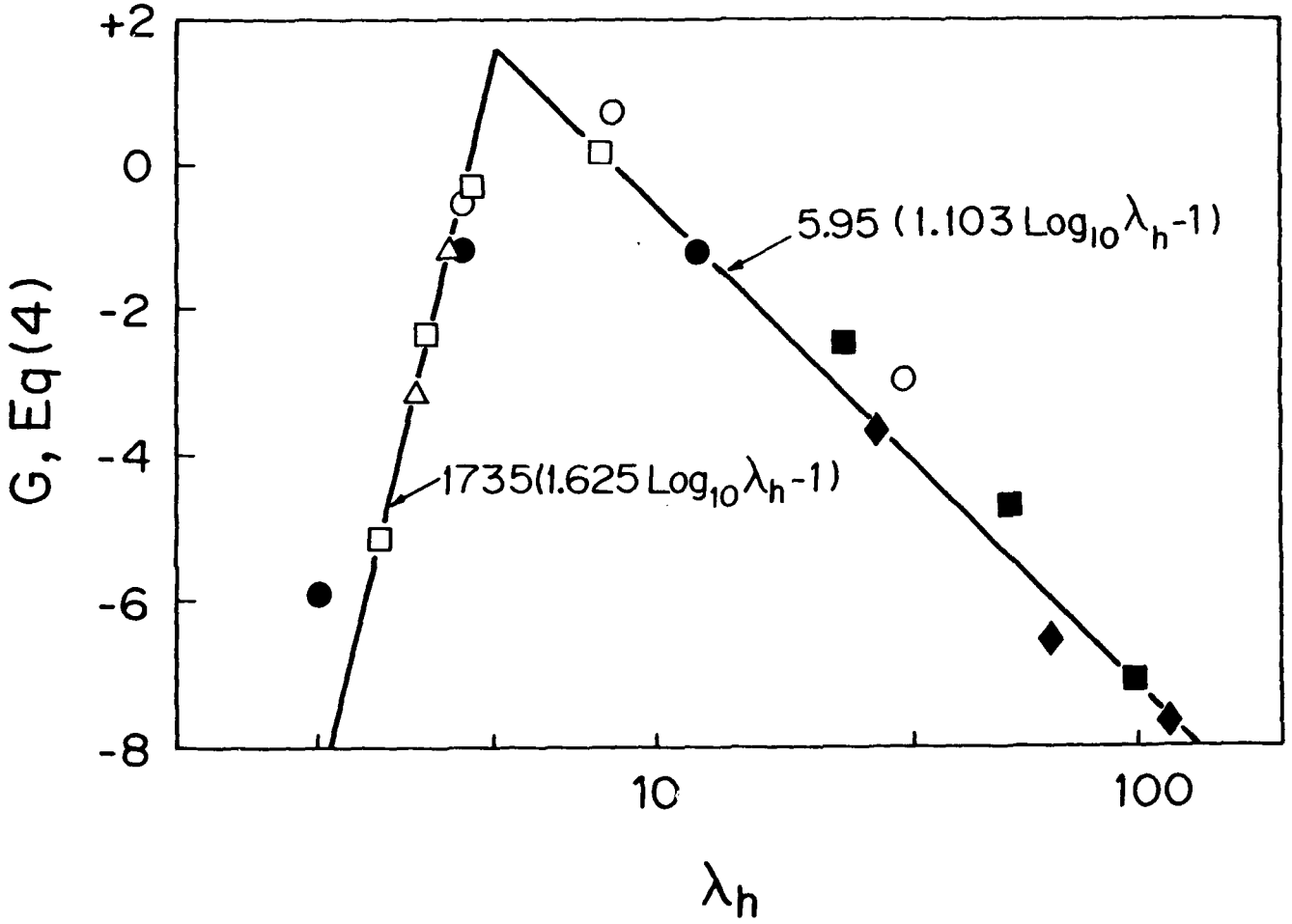

Figure 2. Roughness Effect on the Law of the Wall, Dvorak's Correlation.

The momentum amplification, R_m, in Eq. (5) is considered a parameter that characterizes only a particular type of surface roughness. The variations of R_m with k^+ have been established by Han [12], but only for four types of surface roughnesses. Irrespective of the kind of roughnesses, however, the asymptotic relation of R_m to k^+ is always linear, in keeping with theoretical considerations and experimental findings. This relation may be put as

$$R_m = \beta_m k^+. \tag{7}$$

For the four types of roughnesses analyzed in [12], the values of the coefficients, β_m, are as follows:

Roughness Type	β_m	Range
Nikuradse (sandgrain)	0.3036	$k^+ > 100$
Hama (wirescreens)	0.586	$k^+ > 30$
Moody (random)	0.295	$k^+ > 600$
Colebrook-White (mixed grains)	0.327	$k^+ > 40$

Inserting Eq. (7) into (6) gives

$$\Delta u^+ = (1/K_m)[\mathrm{Log}_e\, k^+ + \mathrm{Log}_e \beta_m]. \tag{8}$$

Inspecting Eqs. (4) and (8), the connection between the linearity coefficient β_m and the intercept constant G is evident. The correlation of Dvorak in Figure 2 can be interpreted as that of the asymptotic coefficient, β_m, with the density factor λ_h vs. G.

Extending Dvorak's work, a more general and useful correlation was developed recently by Dirling [8], who has included in his analysis more experimental data from ablation tests. There are two significant points: one is a more general density factor defined by

$$\lambda_r = (D/k)[A_s/A_p]^{4/3}, \tag{9}$$

where: D = inverse of the square of the number of roughness elements per unit surface area.

k = surface roughness height.

A_s = windward side area of the roughness element.

A_p = projection area of the roughness element in the flow direction.

The definition of λ_r by Eq. (9) encompasses some three-dimensionality effects of the surface roughnesses. A second improvement is that the concept of an equivalent sandgrain roughness is used as the new dependent parameter. It is defined as the sandgrain roughness that produces the same friction as the given surface roughness. Denoting the ratio as (k/k_s), its relation with the intercept constant G can be readily established through Eq. (4a) as

$$(k_s/k) = \exp [K_m(G-G_s)]. \tag{10}$$

The essential difference between Dvorak's correlation and that of Dirling lies in the correlated parameters—the former is on the intercept constant G and the latter is on the equivalent sandgrain roughness ratio. In Eq. (10) it is understood that G = -2.9. By virtue of Eq. (7), the equivalent sandgrain roughness ratio is equal to the ratio of the linearity coefficients, i.e.,

$$(k_s/k) = (\beta_m/\beta_{m\text{-}s}), \tag{11}$$

where $\beta_{m\text{-}s}$ is equal to 0.3036 for Nikuradse's sandgrain.

Dirling's correlation curve is reproduced in Figure 3, in which his two correlation equations for the two sides of the maximum point are, as a result of the present work, replaced by a single equation,

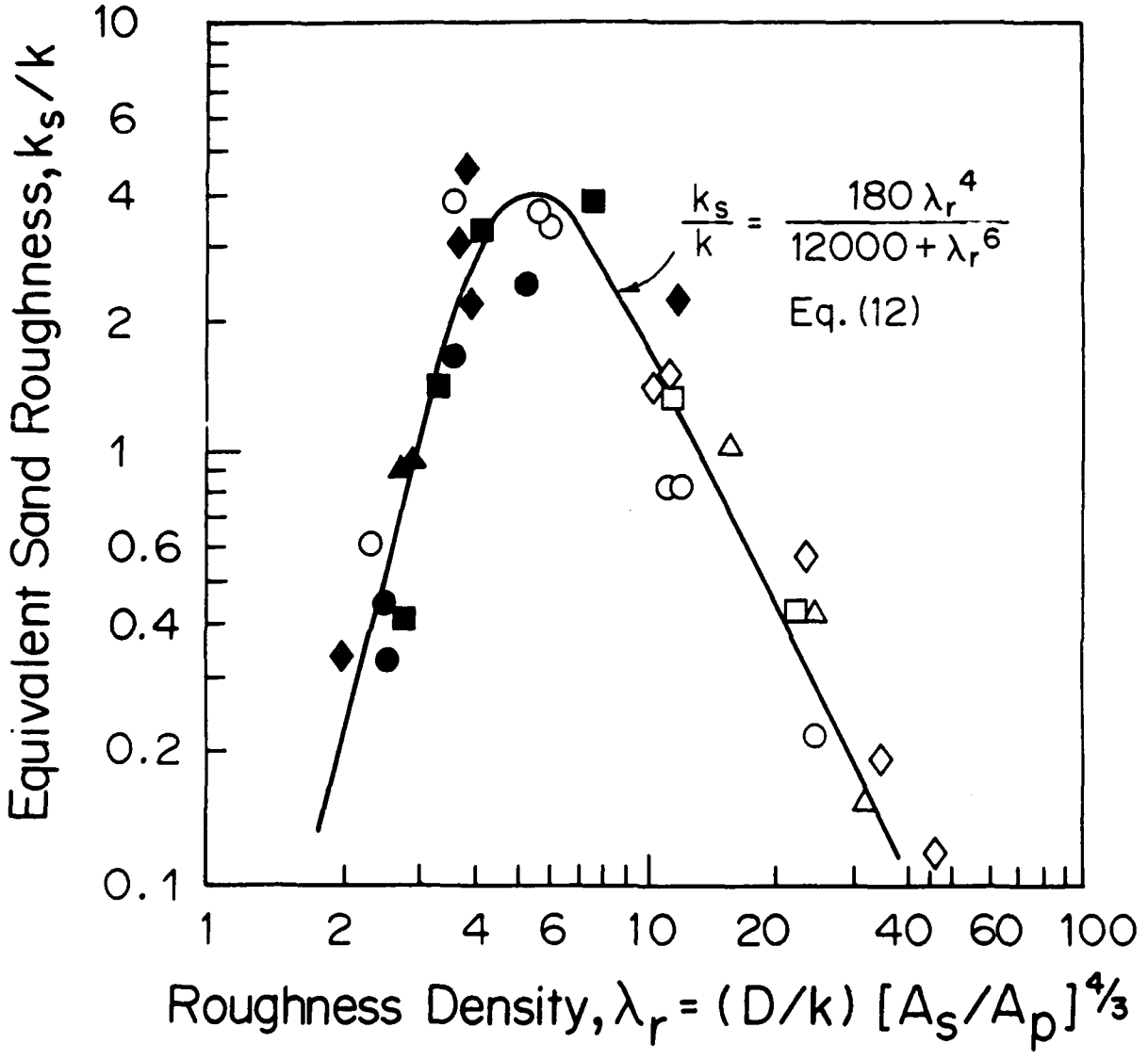

Figure 3. Roughness Effect on the Law of the Wall, Dirling's Correlation.

$$k_s/k = 180\,(\lambda_r)^4/[12000 + (\lambda r)^6]. \qquad (12)$$

From an analytical viewpoint, this equation is much simpler to use. The correlation in Figure 3 includes much recently reported data. It also contains Schlichting's rough surface data [21], which, as they appear in Dirling's original correlation, were, most likely, not yet of a corrected version, according to the work of Coleman, et al. [6].

II.2 Correlation of Roughness Density: Transition-Region Relation

For intermediate values of k^+, the downshift Δu^+ should be given by Eq. (6), in which an analytical representation of R_m in terms of k^+ is desirable. The starting point is the numerical tabulations of R_m vs. k^+ available in [12] for the four roughnesses previously mentioned. Of these, those of Hama and Nikuradse are more typical of aerospace applications. The following expression was found to be a fair representation of the R_m-k^+ relation in general:

$$R_m = \beta_m\,(k^+)^3/[10^5 + (k^+)^4]^{1/2}. \qquad (13)$$

Eq. (13) has only one free parameter, β_m, which is the characteristic slope for a particular type of roughness. The usefulness of Eq. (13) lies in its ability to reproduce the numerical values of Δu^+ on which values of R_m's are based. To test the compatibility, Eqs. (6) and (13) are merged to calculate Δu^+, using two values for β_m: those of Hama's wirescreens and Nikuradse's sandgrain. For the former, the computed Δu^+ and the experimental input data are shown together in Figure 4 in which satisfactory agreement is observed. A similar conclusion can be said of Nikuradse's data (not shown in Figure 4).

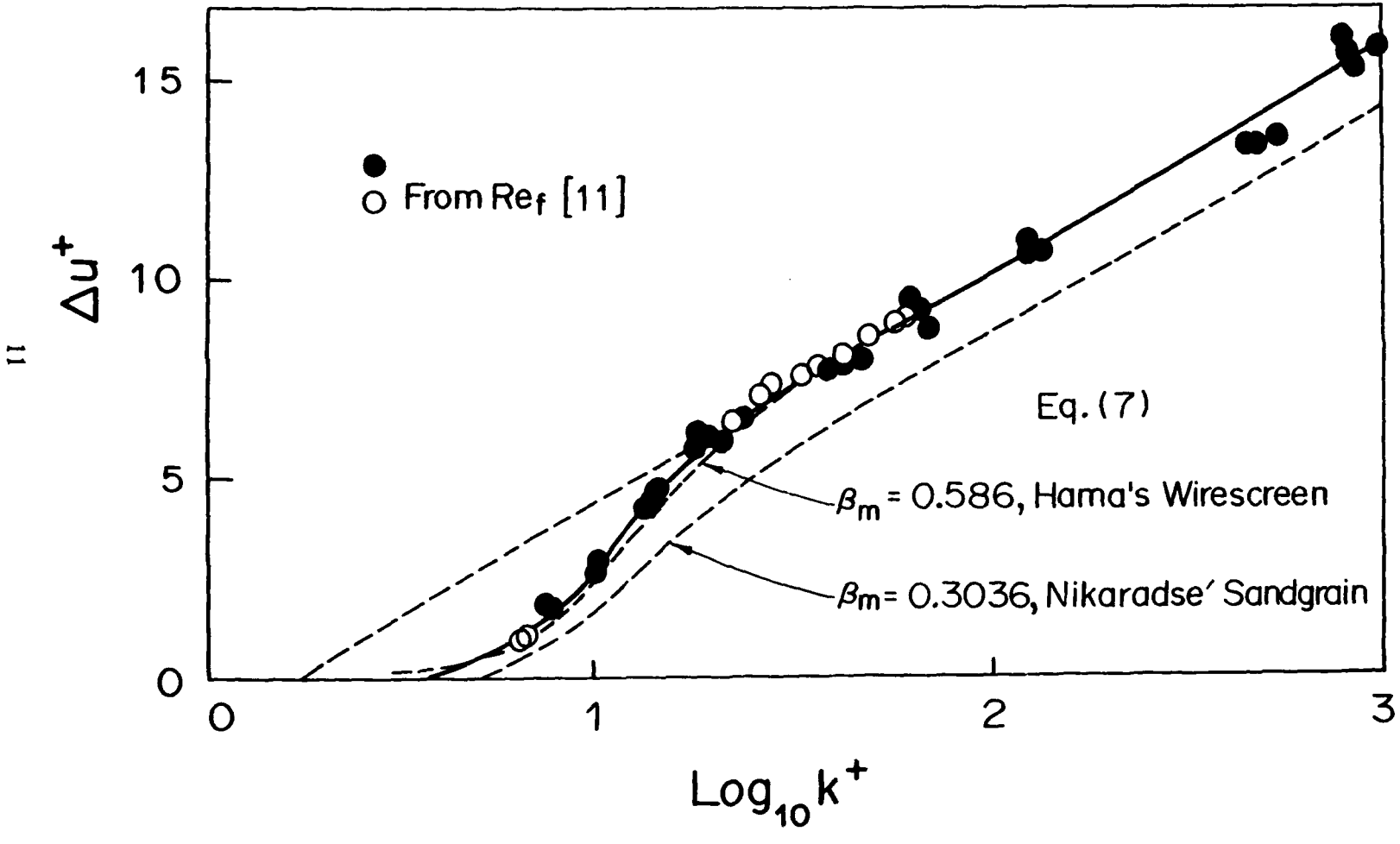

Figure 4. Comparison of Calculated and Measured Velocity Shifts.

III. AN EXPERIMENTAL INVESTIGATION OF THE SURFACE ROUGHNESS EFFECTS ON TURBINE AIRFOIL WAKES

Several experimental programs have measured the compressor efficiencies with compressor blade surfaces artificially roughened. Evidence of the reduced performance justified the conclusion that it is the surface roughness that leads to an increased momentum thickness, which eventually deteriorates the compressor efficiencies with lowered flow rates and less pressure ratios than otherwise. For turbine applications, a direct fluid dynamic consequence is the altered wake velocity profiles experienced by first-stage turbine airfoils. The altered wake profiles may be the result of surface erosion of the upstream nozzles. Thus, an experimental demonstration of this effect is of value in assessing the wake-cutting phenomenon in turbine performance analysis. We should note that this part of the present work is only concerned with the wake flow phenomenon as influenced by surface roughness and does not address the effect of heat transfer augmentation due to surface roughness.

III.1 Test Facility and Instrumentation

An open circuit wind tunnel with a test section of 61 cm vertical and 46 cm horizontal was used to conduct the experiment. Two damping screens were installed at the entrance and at the end of the contraction section of the tunnel to reduce the turbulence level in the test section. Reduction of the turbulence level in the tunnel was particularly important since the disturbances contributed by the rough elements are easier to identify at the lower freestream turbulence. The velocity pattern was ascertained to be uniform with 1% overshoot near the center of the tunnel. A total Pitot tube made of a hypodermic needle of 0.30 mm inside diameter and 0.60 mm outside diameter was used to measure the mean velocities in the wake. The freestream turbulence level of the test section was measured by a hot wire anemometer and was found to be about 1%. The hot wire was a constant temperature, single wire, with a tungsten sensor wire of 1.27 mm in length and 0.0038 mm in diameter. A linearizer circuit was used to obtain a linear output for the hot wire to achieve maximum accuracy in turbulence measurements. Signals from the anemometer were fed into a

cross channel spectrum analyzer. An averaging process was used to obtain the frequency spectra and total turbulence intensity for each location in the flow.

A symmetrical airfoil of NACA0015, scaled to a chord length of 178 mm and a camber of 27 mm, was positioned in the center of the test section. The air speed was kept at 20.7 m/sec at one atmosphere and room temperature. The airfoil chord Reynolds number was therefore 233,000 for all runs. Surface roughness was provided by gluing sandpapers of commercial grades over the entire surface of the airfoil. In this way, symmetry of the roughness pattern was achieved. In surface roughnesses, the largest particles usually have a more significant effect on destabilizing the boundary layers; therefore, the designation representing a roughness must give some indication on the maximum size of the particles. To evaluate the corresponding roughness sizes of the sandpapers, American National Standard Institute (ANSI) specifications for the grading of abrasive grains was consulted. The roughness values expressed in terms of the ratio of the average protrusion size to the airfoil chord and roughness Reynolds number based on 20.7 m/sec freestream velocity are summarized in the following table.

Roughnesses Used in the Experiment

Grit No.	k, mm	$(k/L)10^3$	Re_k
150	0.133	0.748	174
80	0.336	1.889	440
50	0.551	3.099	722
36	0.780	4.387	1022

III.2 Experimental Results

Overall Characteristics of the Wake

Velocity profiles in the wake were obtained at three different distances downstream of the airfoil for the five different surface conditions. Symmetry of the wake was checked and found to be acceptable. Therefore, the velocity profiles are only plotted for one half of the wake and are shown in Figures 5 through 9. Each one of these figures shows the wake velocity profiles at three

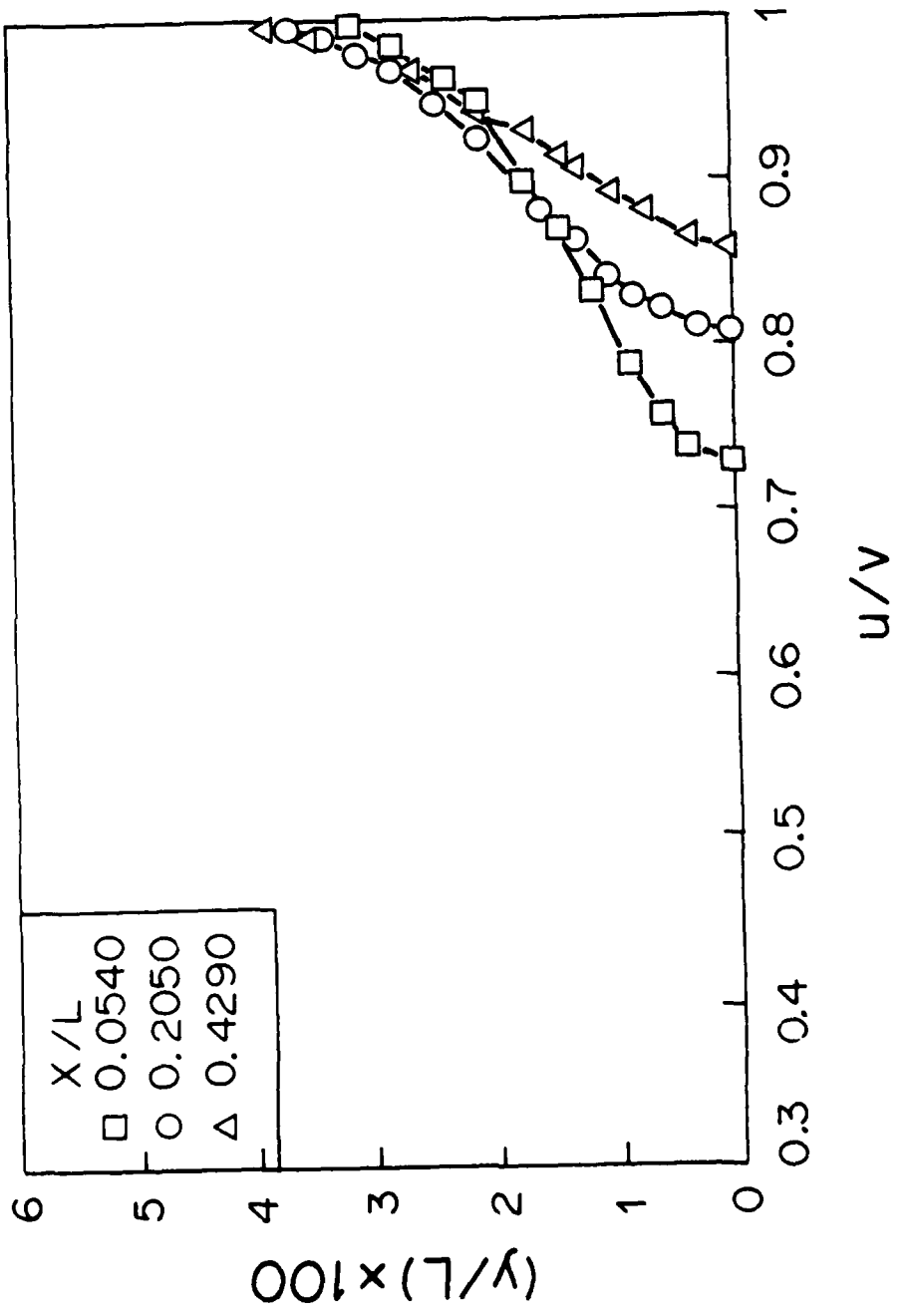

Figure 5. Wake Velocity Distributions, Smooth Surface.

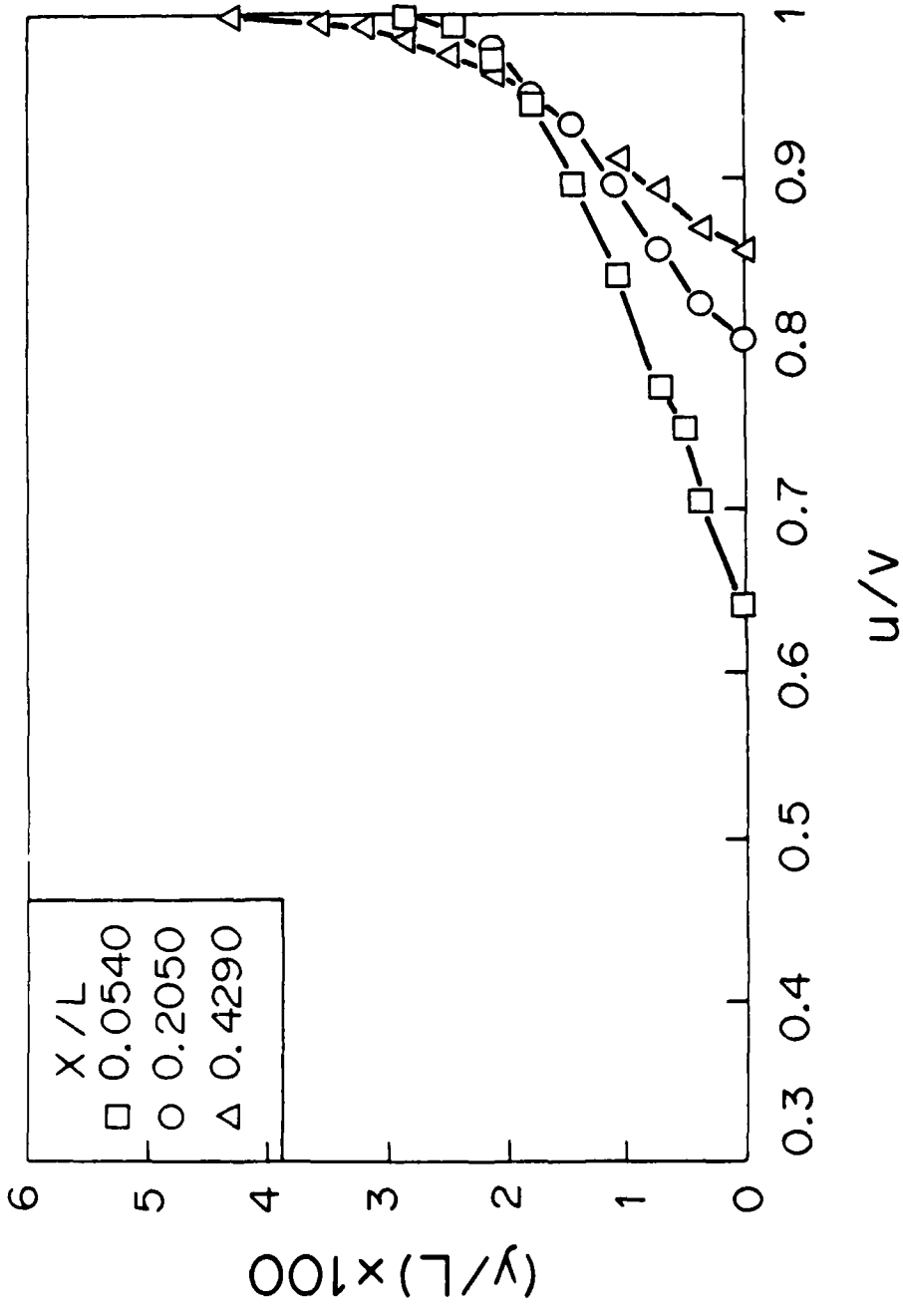

Figure 6. Wake Velocity Distnbutions, $Re_L = 174$

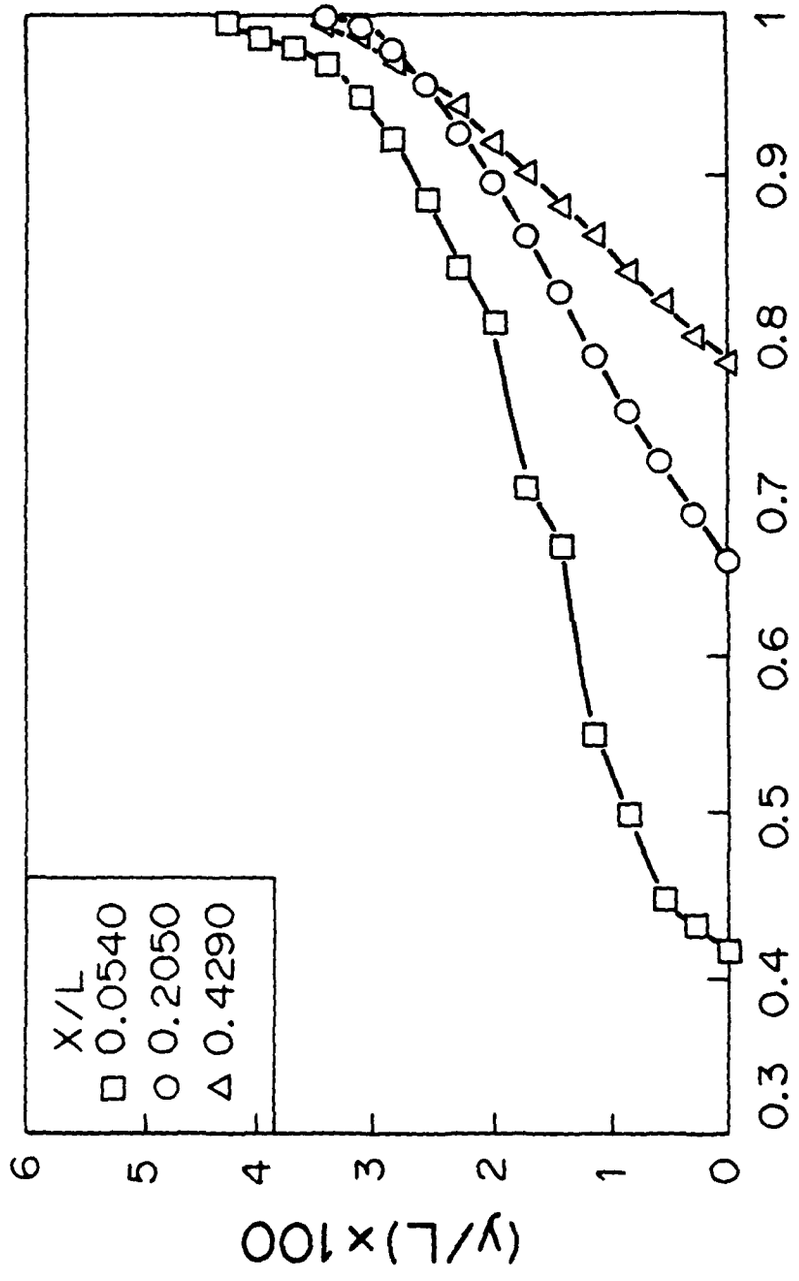

Figure 7. Wake Velocity Distributions, $Re_x = 440$

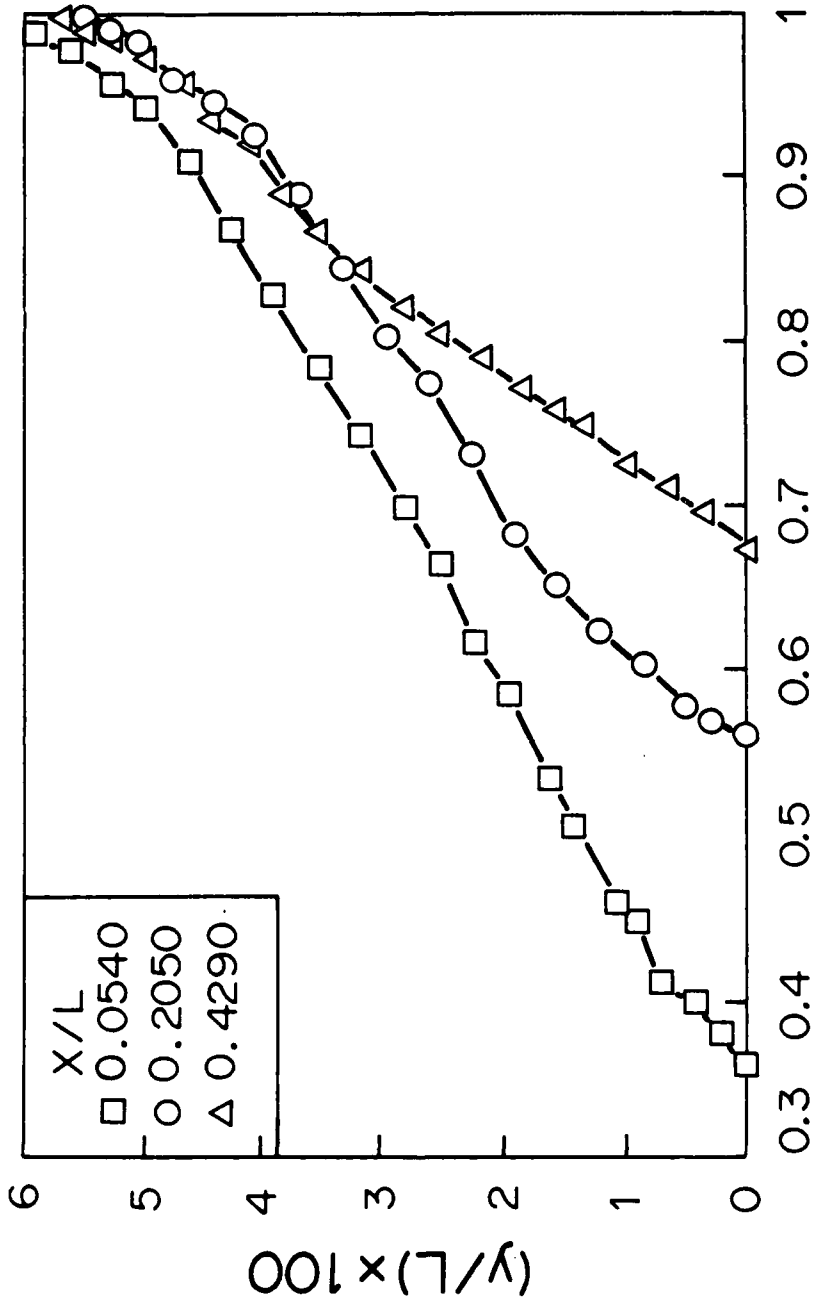

Figure 8. Wake Velocity Distributions, $Re_L = 722$

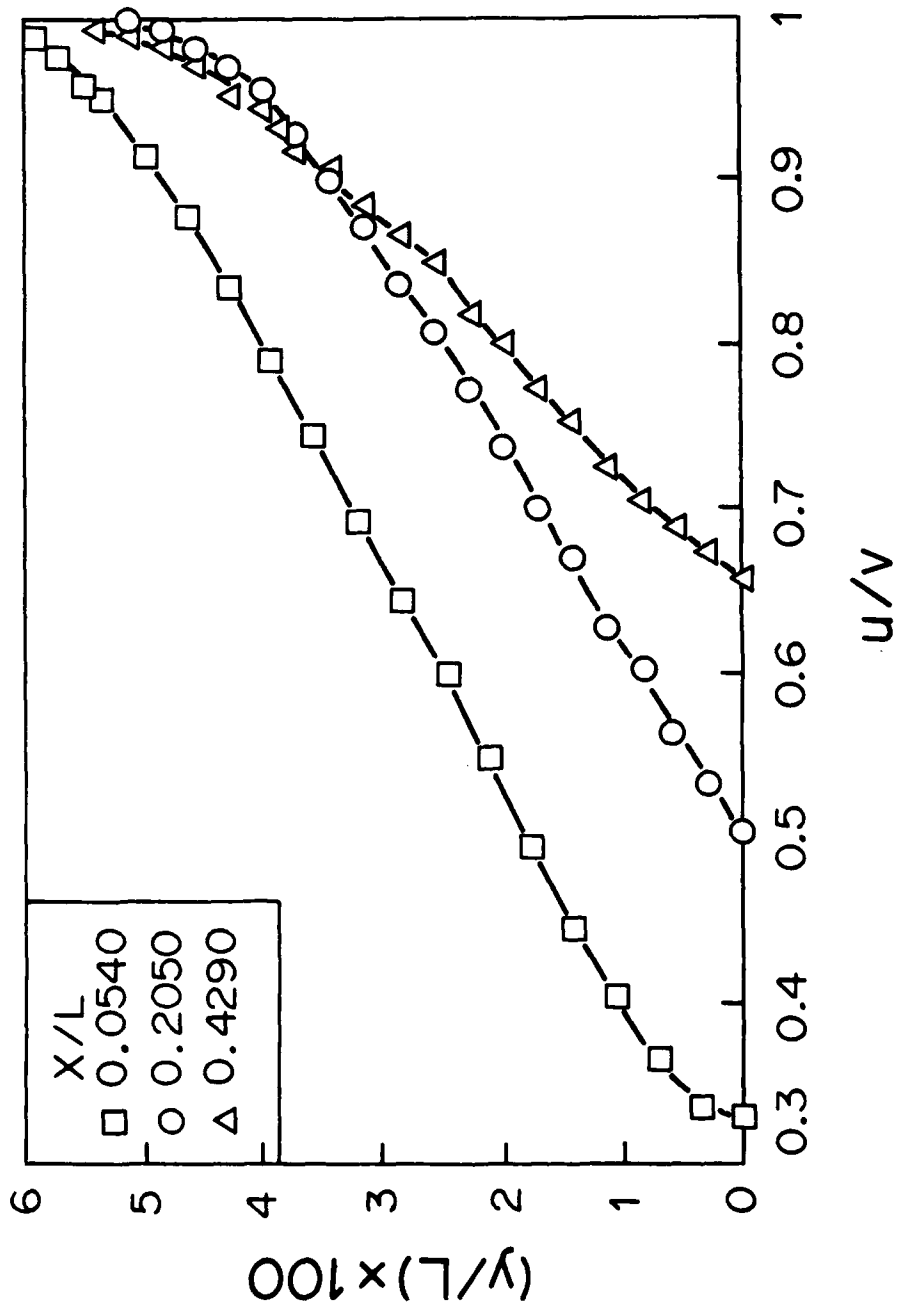

Figure 9. Wake Velocity Distributions, Re_x = 1022

different downstream locations for a specific surface roughness. Figure 5 is for the smooth airfoil, and the succeeding figures are for progressively rougher surface conditions. Comparison between these figures indicated that the width of the wake at a given streamwise location increases with increasing surface roughness. One observation is that for the three rougher cases for which the profiles are in Figures 7, 8, and 9, the wake widths decrease with the distance from the trailing edge. In the case of the other two wake profiles, Figures 5 and 6, for less rough surfaces, the trend of decreasing wake width is not apparent. The effect of surface roughness is to produce a boundary layer with a greater thickness on a rough airfoil compared to that of a smooth airfoil. With the trailing edge boundary layer profiles as the starting profile in the developing wake region, there would be a greater entrainment from the outer stream to the wake of a rough wall compared to that of a smooth wall. This may be responsible for the trend of decreasing wake width in the near wake region. Farther away from the trailing edge, where the wake is independent of the aerodynamic loading of the airfoil, the wake width is expected to resume its increase in the streamwise direction.

The momentum thicknesses for each roughness condition were measured at three streamwise locations inside the wake and are plotted in Figure 10. This figure shows that the momentum thickness, which is an indication of the loss of fluid momentum, is increasing with roughness. Theoretically, the momentum thickness should remain constant throughout the wake. Higher values of the momentum thickness close to the trailing edge are due to the lack of static pressure recovery in that region. Downstream from the trailing edge, constancy of the momentum thickness is an indication of the self-preservation of the flow and static pressure recovery. Figure 11 shows the momentum thickness variation with roughness Reynolds number and compares the measured values with those calculated at the trailing of a flat plate at the same Reynolds number. The measured momentum thicknesses in Figure 11 are those at a sufficient distance (X/L=0.43) away from the trailing edge of the airfoil where momentum constancy is established. Figure 11 can be divided into three sections. Zone one shows a near equality in the values of the measured and calculated momentum thickness. This range of low roughnesses could be defined as the limit

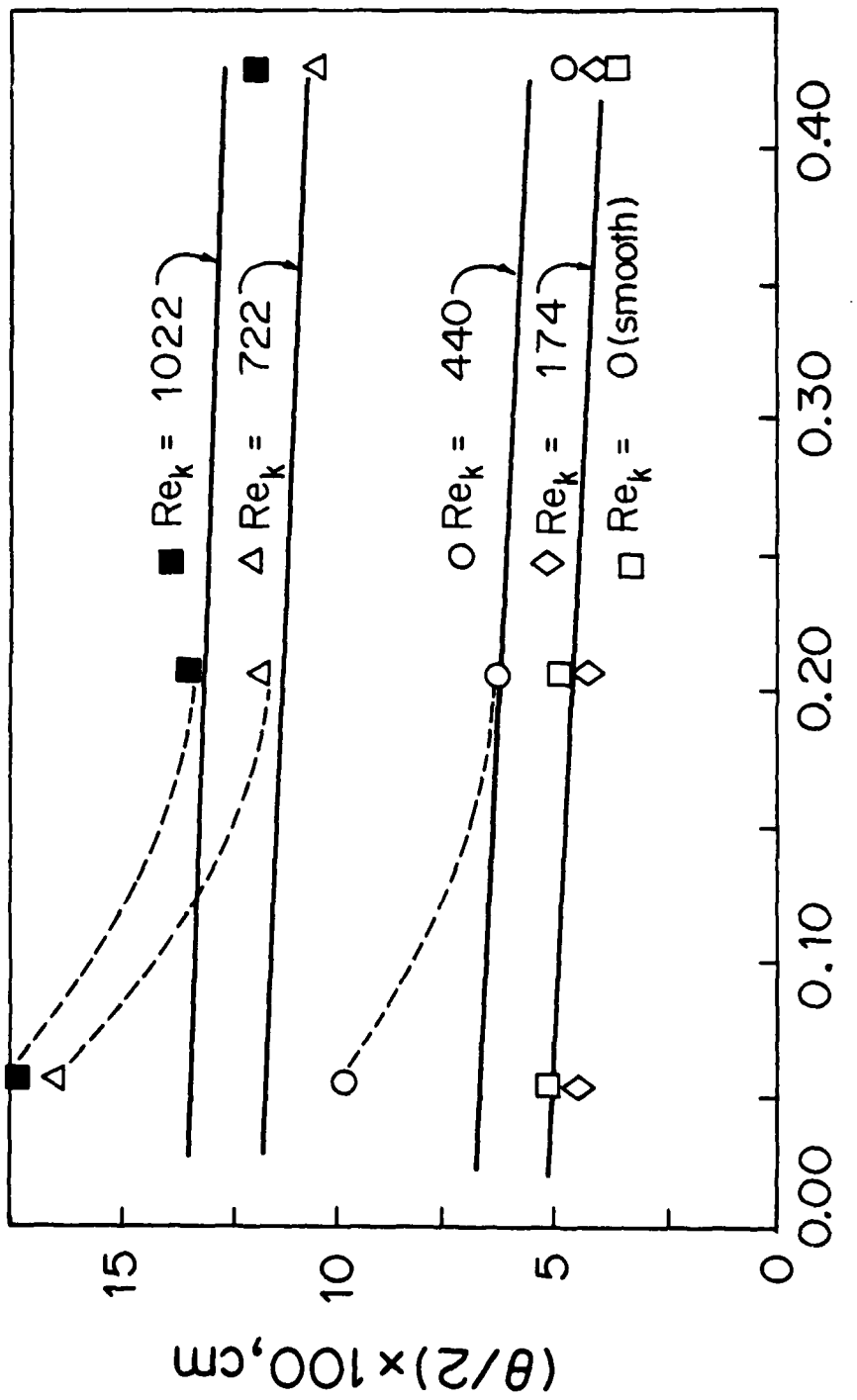

Figure 10. Measured Momentum Thickness Variations.

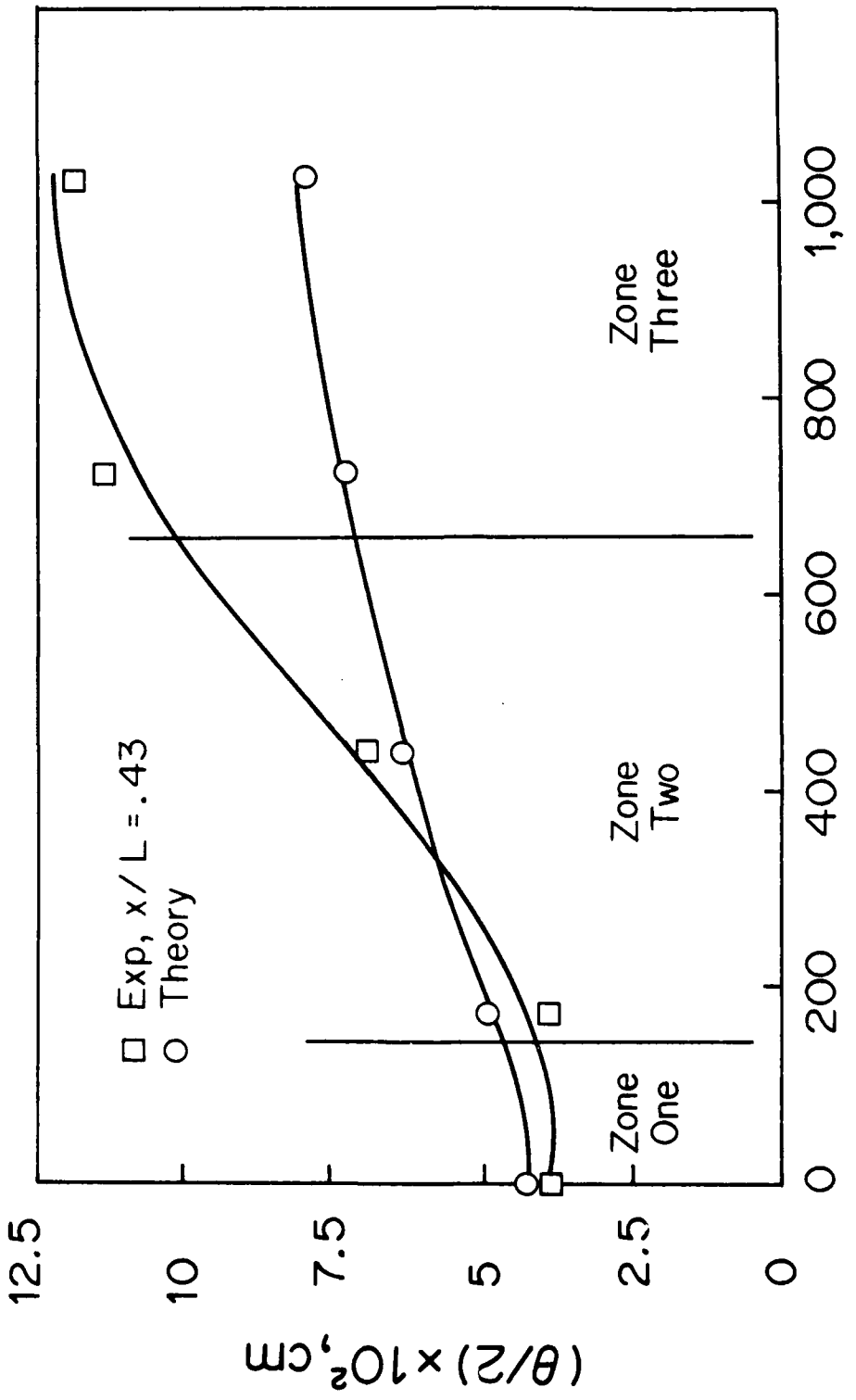

Figure 11. Momentum Thickness vs. Roughness.

of tolerable roughness (or hydraulically smooth) in which the size of the roughness elements has no significant effect on the wake characteristics. Further increase in the average height of the rough elements results in a sharp increase in the momentum thickness, as shown in zone two of Figure 11. The third zone of the curves indicates a much slower increase in the momentum thickness as a consequence of an increase in the roughness. Unfortunately, theoretical predictions are not in accord with measured values. Therefore, it appears that a smaller increase in the average height of the roughness elements, beyond a tolerable roughness, has a more significant effect on the increase in the drag of the body. Bammert [1] studied the influence of the blade surface roughness on the efficiency of gas turbines. Their observations indicated that the rate of drop in turbine efficiency decreased with the increase of surface roughness. This is in line with the conclusion of this study.

Figure 12 shows the variation of the shape factor in the streamwise direction. The shape factor increases with the surface roughness. Further downstream, where the wake becomes self-preserved and independent of the airfoil, the shape factor should approach unity, and this seems to be the trend in Figure 12.

An important characteristic of the flow in a symmetrical wake is the centerline velocity variation with the distance from the trailing edge. For the five roughnesses investigated, the variations of the centerline velocity with X/L are shown in Figure 13.

Most significant is that for the smoother airfoils, the centerline velocity recovery is much faster than for the rougher airfoils. Since the wake deficit or the displacement thickness is an indication of the needed flow entrainment, it follows that for smooth walls producing smaller displacement thicknesses, the centerline velocity can recover much more rapidly than for rough walls. As these different recovery processes continue, the wake profiles for the five cases gradually merge into a single shape, indicating vanishing effects of upstream conditions. The measured centerline velocities in Figure 13 do not match the calculated velocities, though the trend is correct. To correlate the effect of the roughness size on the centerline velocity recovery, the streamwise distance is normalized by the momentum thickness measured for each corresponding

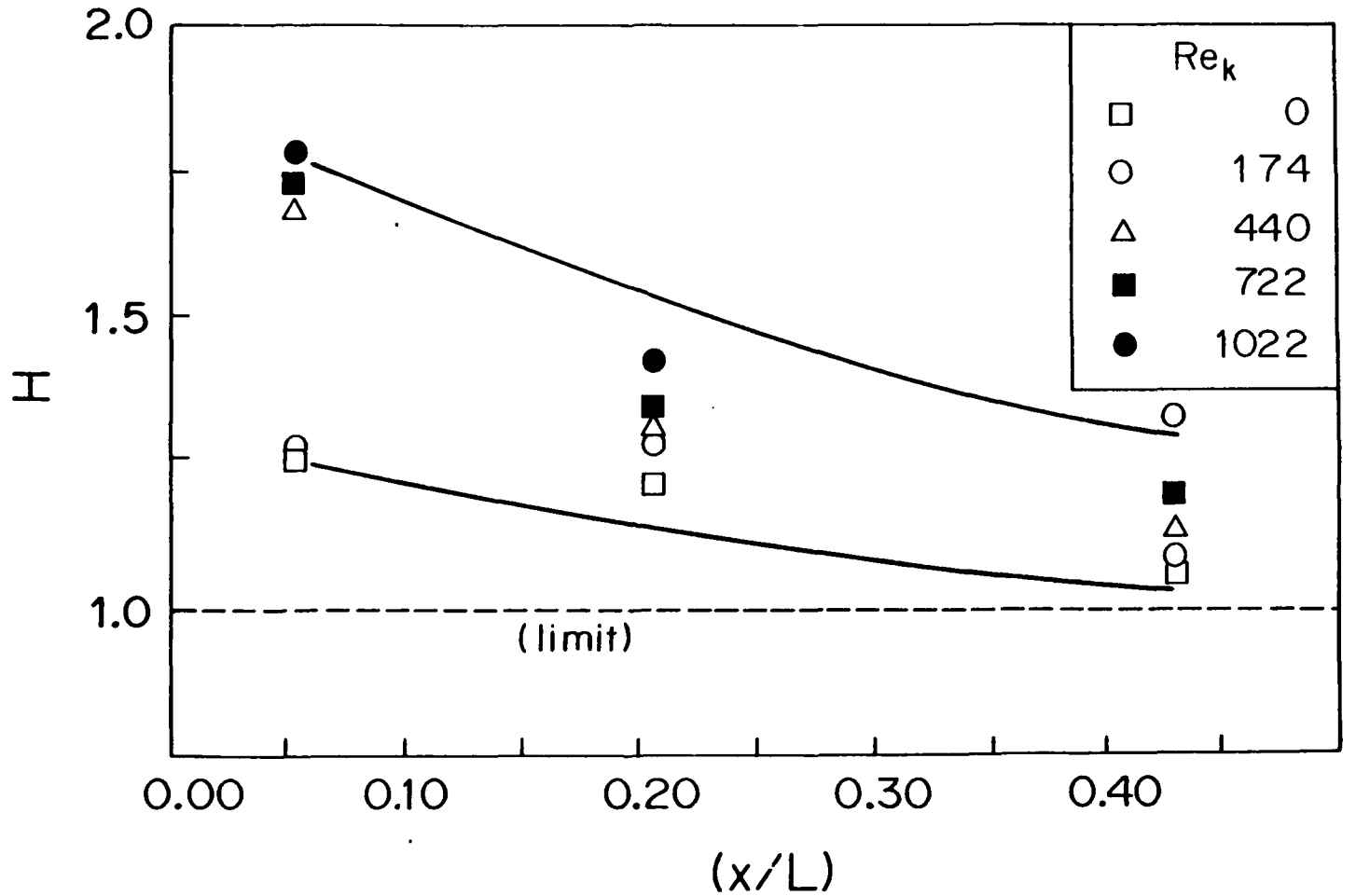

Figure 12. Shape Factor Variations in the Streamwise Direction.

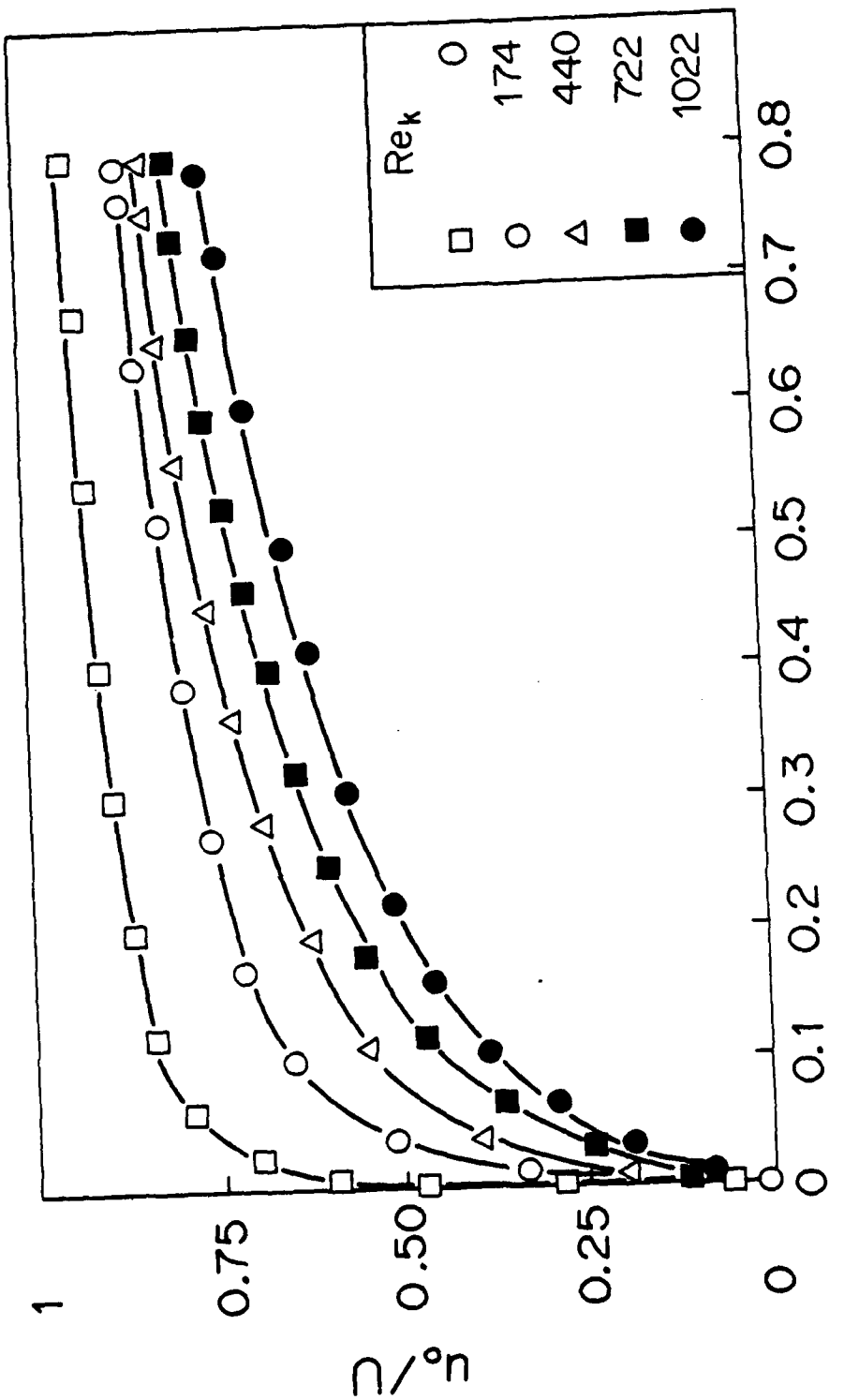

Figure 13. Experimental Centerline Velocities in Wakes.

roughness. Figure 14 shows the calculated wake centerline velocity variations with the normalized streamwise distance ($x\theta_o/L\theta$), where θ_o is the starting momentum thickness. The values of θ used in the construction of Figure 14 were those measured in this series of experiments. From this figure, it appears that the surface roughness effects are well represented by the nondimensional distance (x/θ), since all calculated points are merged into a single curve. To further validate the correlation, a parallel construction was shown in Figure 15, where the measured velocities were used. The resulting pattern of distribution is not consistent with that in Figure 14. Only in the far wake region, i.e., at large values of x, do different data points gradually converge towards a single curve. This is where the flow becomes self-similar, as is well established experimentally and theoretically.

Turbulence Properties

Flow over a single roughness element is known to result in separation bubbles that at high Reynolds numbers are transformed into continuous vortex shedding. The frequency and scale of the generated vortices are therefore a function of the roughness size and the flow Reynolds number. It follows that turbulent wakes behind a rough airfoil are comprised of eddies of different sizes and traveling with various frequencies.

In this work, a detailed analysis of the frequency spectra in the wakes was carried by a hot wire anamometer and wave analyzer. In all cases, no peak components at a selected frequency were found in the wake. Because of the random nature of the roughness elements in size and distribution, flow disturbances in the boundary layer with a particular frequency will have its energy spread across the entire frequency spectrum. This is partially confirmed by the measured data of the streamwise turbulent fluctuations. At the wake symmetry line and for three roughness Reynolds numbers of 174, 722, and 1022, the rms-amplitude frequency spectra are shown in Figures 16, 17, and 18. Of significance is that the amplitude of the low-frequency disturbances decreases along the streamwise direction, while some of the high-frequency ones show an opposite effect, e.g., at 1,500 Hz and above.

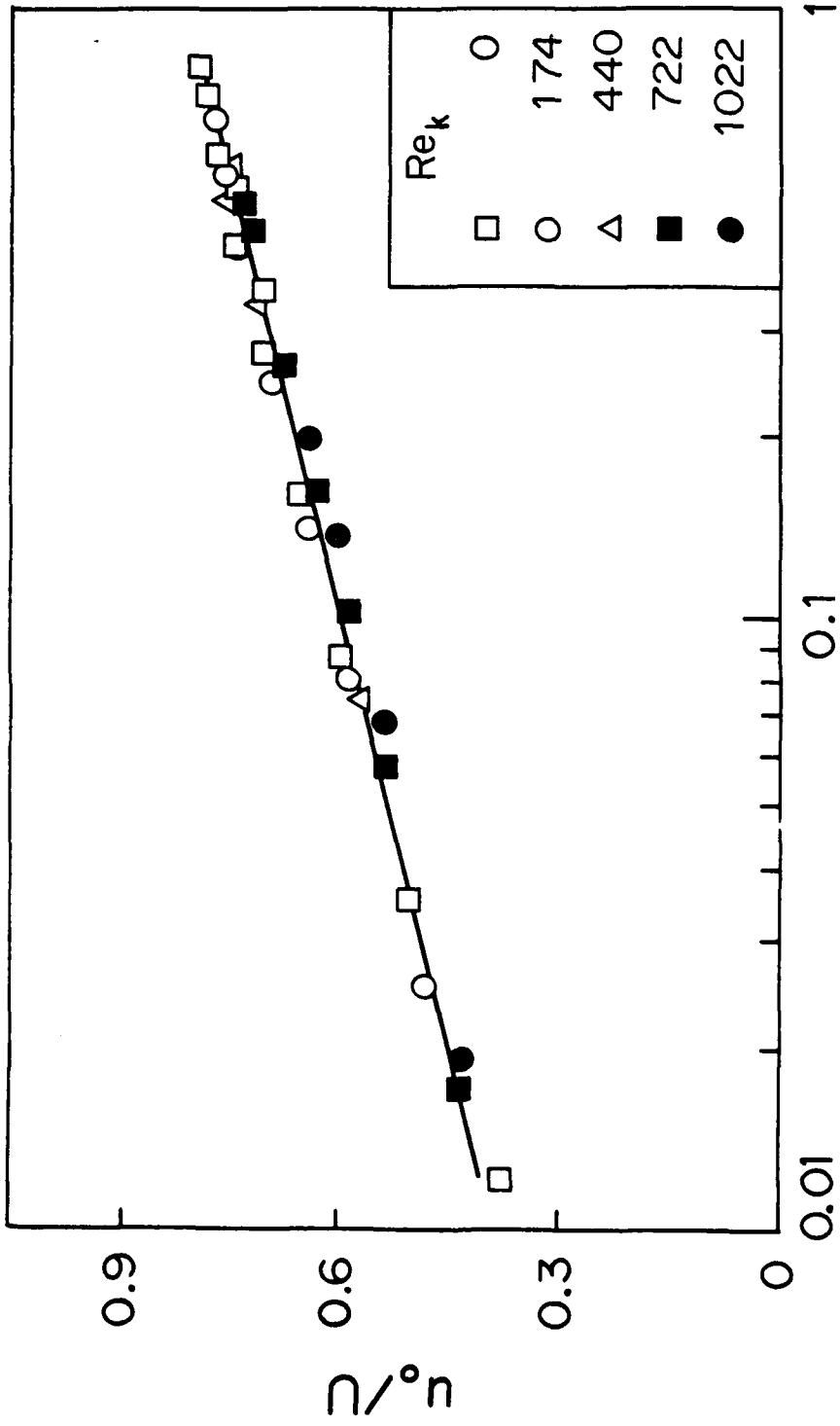

Figure 14. Normalized Centerline Velocities, Calculated.

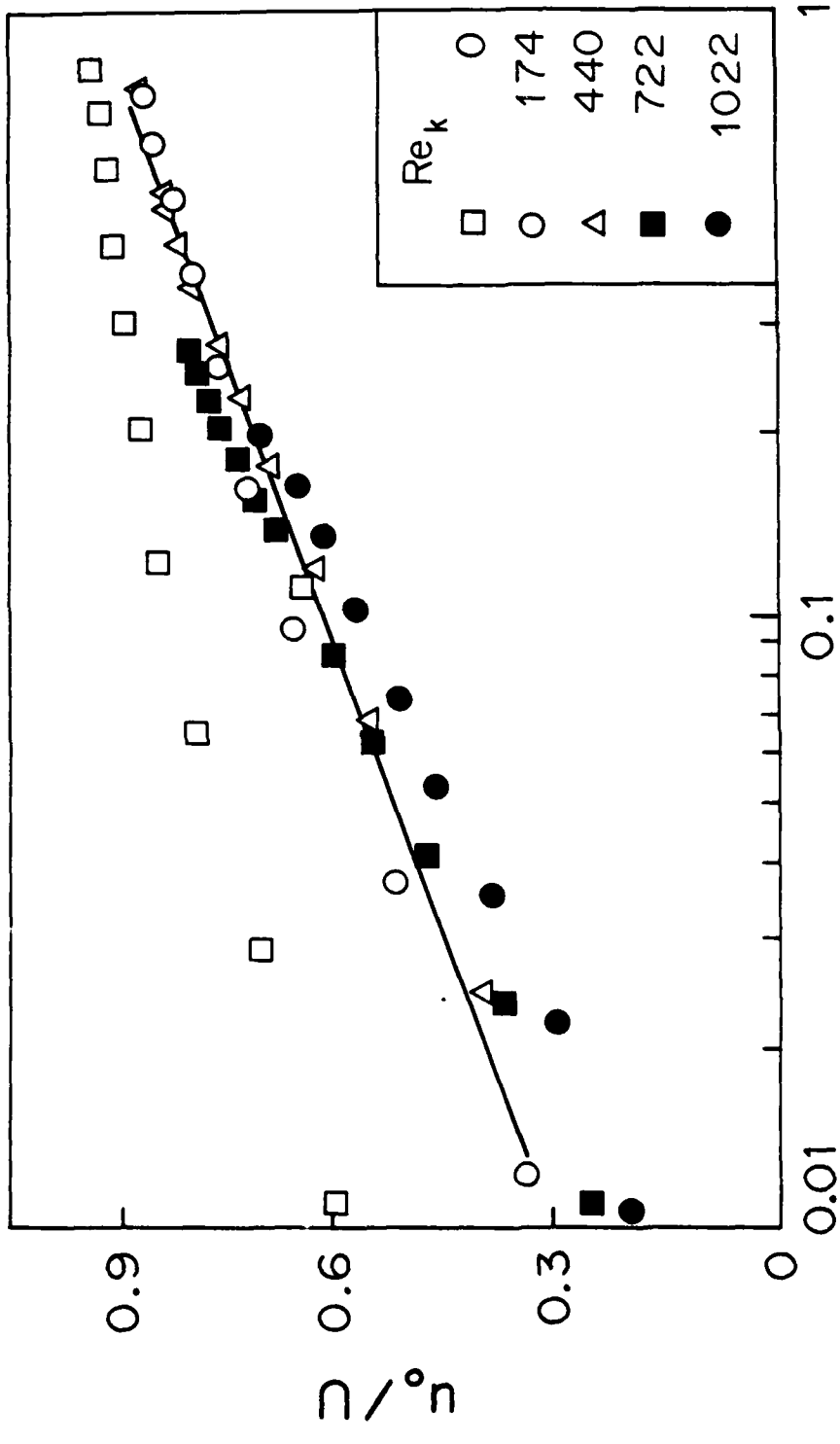

Figure 15. Normalized Centerline Velocities, Experimental.

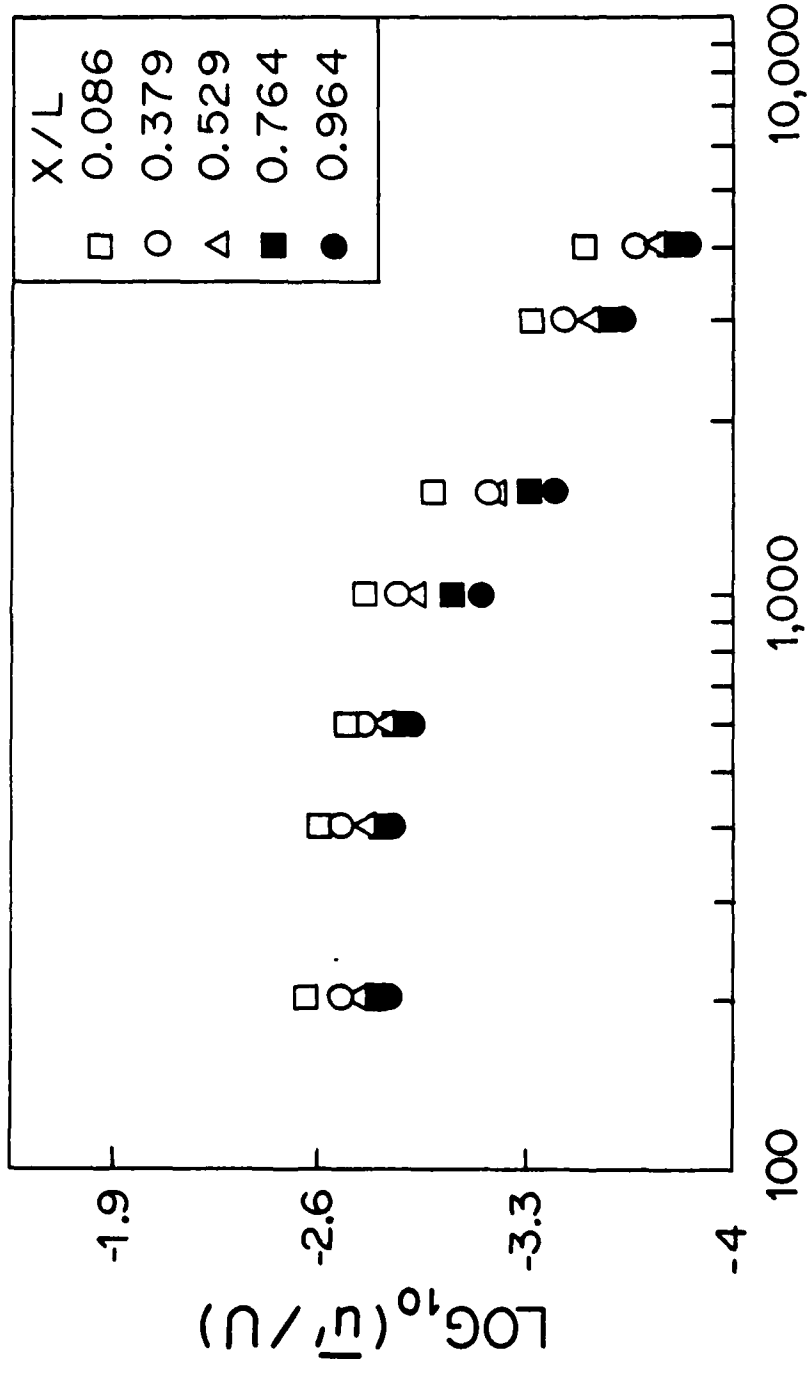

Figure 16. Streamwise Fluctuation Spectra at Centerline, $Re_k = 174$

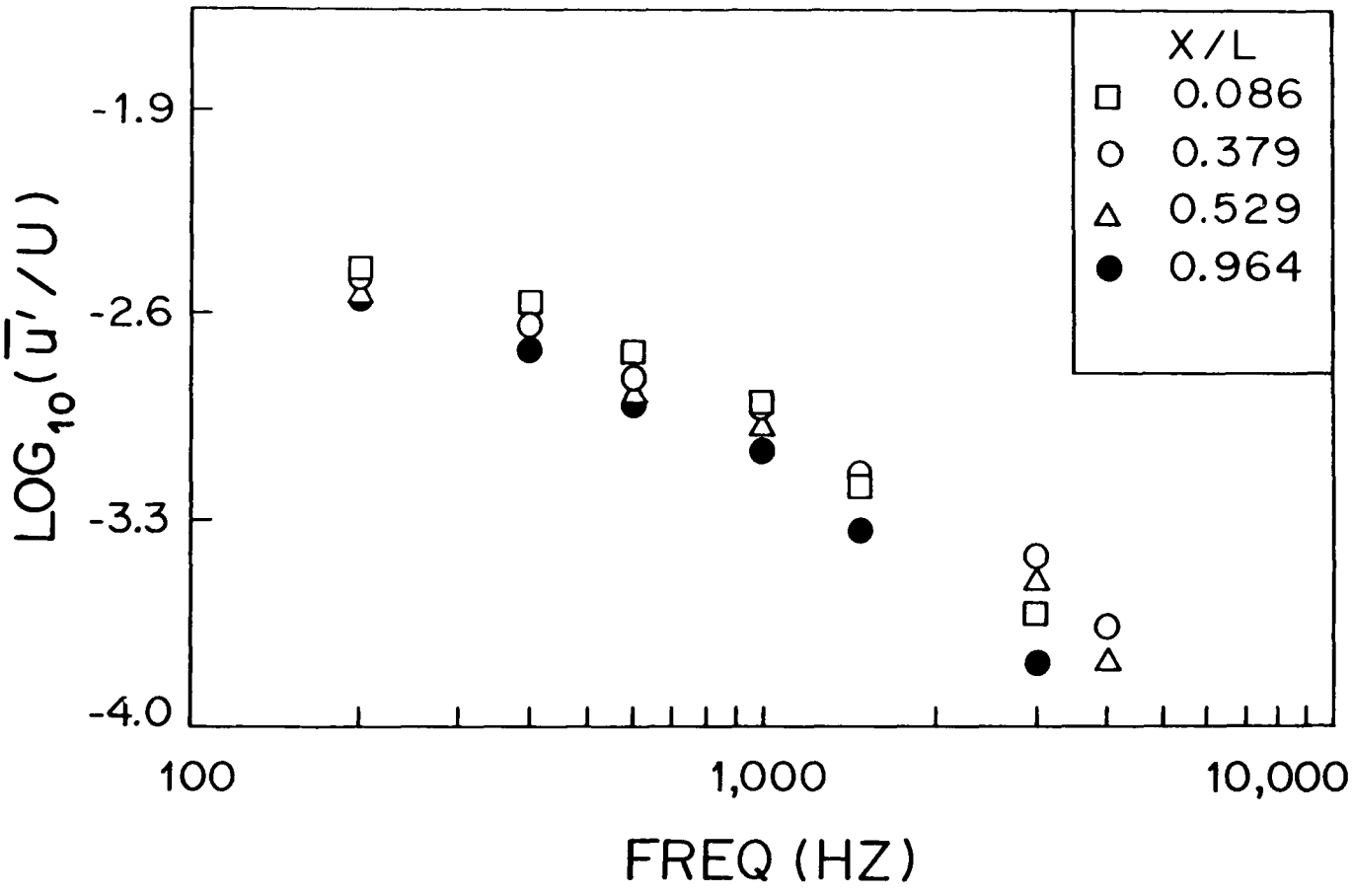

Figure 17. Streamwise Fluctuation Spectra at Centerline, Re_t = 722

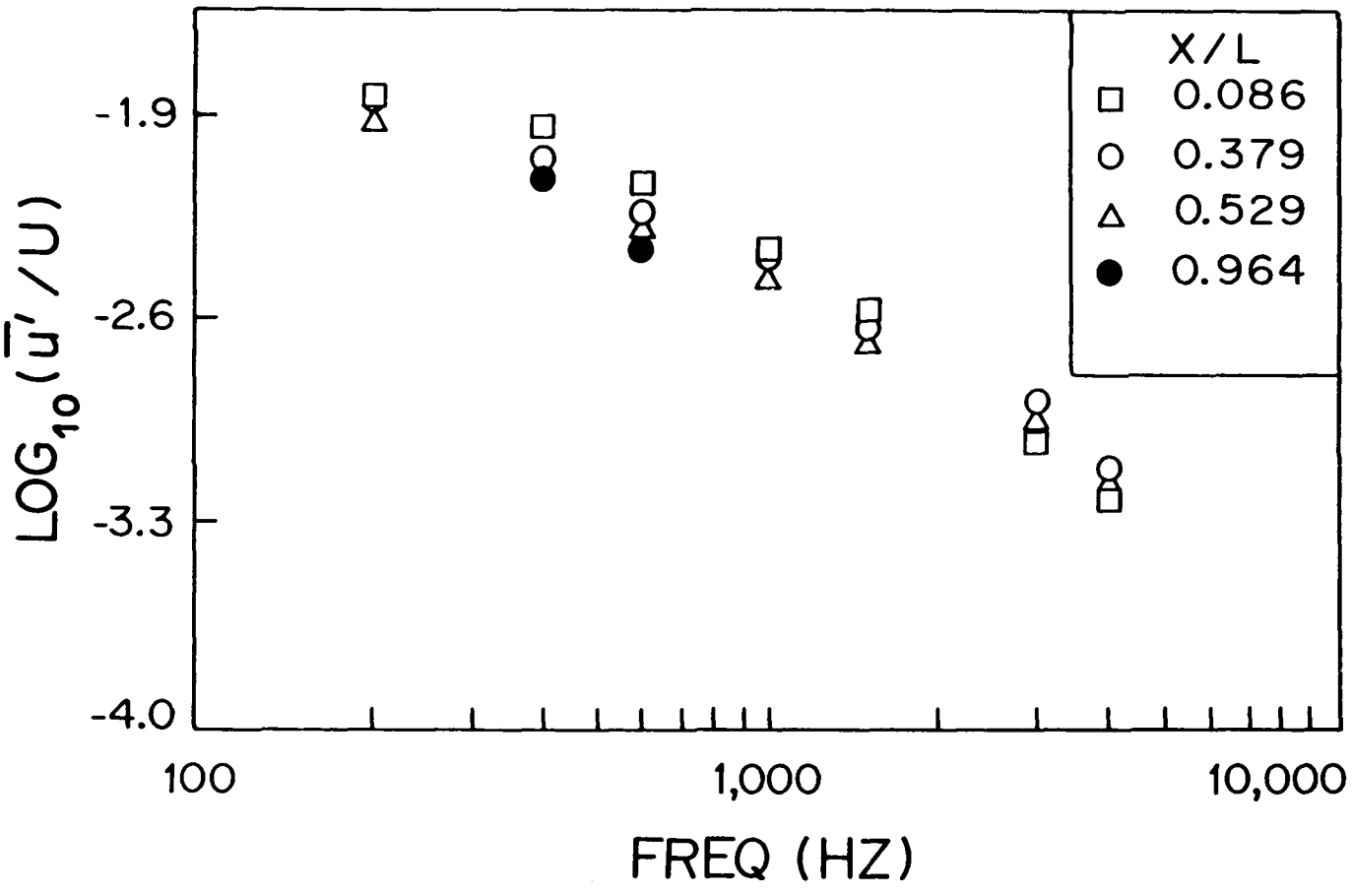

Figure 18. Streamwise Fluctuation Spectra at Centerline, Re_k = 1022

Figure 19 displays the maximum turbulence intensity at each wake cross section as a function of the roughness Reynolds number for five wake stations. At each axial distance characterized by the symbol, the maximum intensity increases with increasing surface roughnesses—at high rates for low roughnesses. It appears that the data pointed towards a plateau value at high roughnesses. Of particular interest is that, at low roughnesses, the maximum intensity decays in the stream direction at higher rates for low roughnesses than for higher roughnesses. For the later case, turbulent flow prediction models based on a constant viscosity model appear conceptually justified.

On a finer scale, the turbulence intensity distributions in the normal direction are shown in Figures 19 and 20 for two wake positions. Data in Figure 19 indicate that the maximum intensity occurred at the wake center line, except that for a smooth surface for which the turbulence is zero on the wall at the trailing edge. The convected profile at a small distance of $x/L = 0.38$ still retains the general shape convected from the trailing edge. However, for rough surfaces, the initial shape emanating from the trailing edge has a maximum at the surface which becomes the wake symmetry line. That a maximum intensity occurs at the surface—provided the roughness is above a critical value—produces the distribution curves as indicated. Progressing into the wake, the symmetry line becomes a region of zero shear, and the peak intensity point moves away from the center, as Figure 21 testifies. In both figures, the intensity decays to the freestream value at large transverse positions. In this outer region, the intensity distribution shapes follow a scaling rule shown in Figure 22, where the intensity is normalized by the maximum intensity with the freestream value as the base. The data points, although not merged into a single curve, appeared to form a narrow band, indicating a self-preserved structure. That this should appear so is readily explained based on a one-dimensional (transverse) diffusion of the intensity while the advection effects are of negligible consequence.

The implications of the experimental results as applied to turbine airfoil heat transfer are self-evident. If the stationary vanes have rough surfaces, their wakes would contain a higher velocity deficit and high turbulence intensities. For the first-stage turbine blades cutting across

these wakes, the stagnation heat transfer would be greatly increased by these two factors, even if the blade surfaces were to remain smooth.

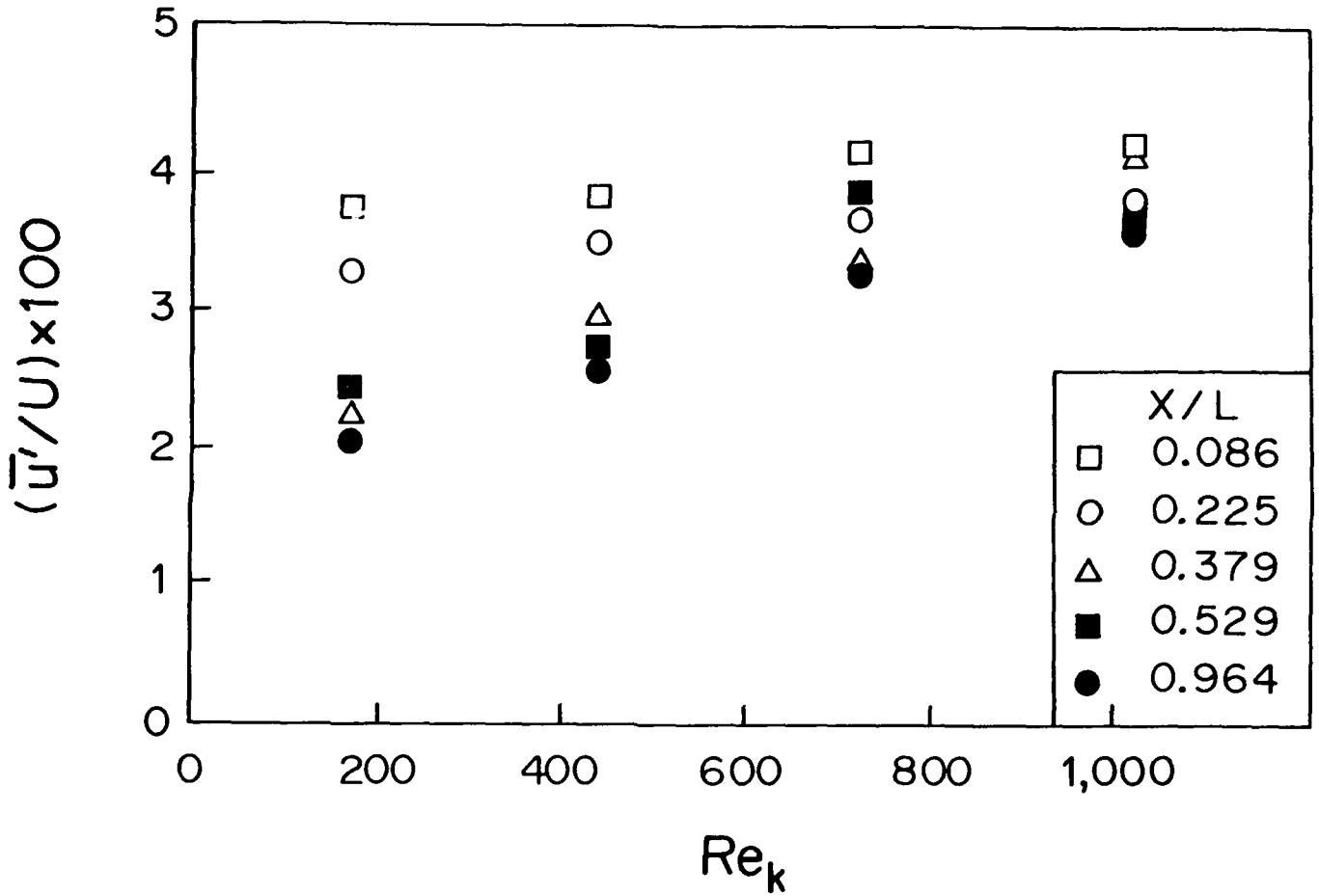

Figure 19. Maximum Turbulence Intensities in Wakes.

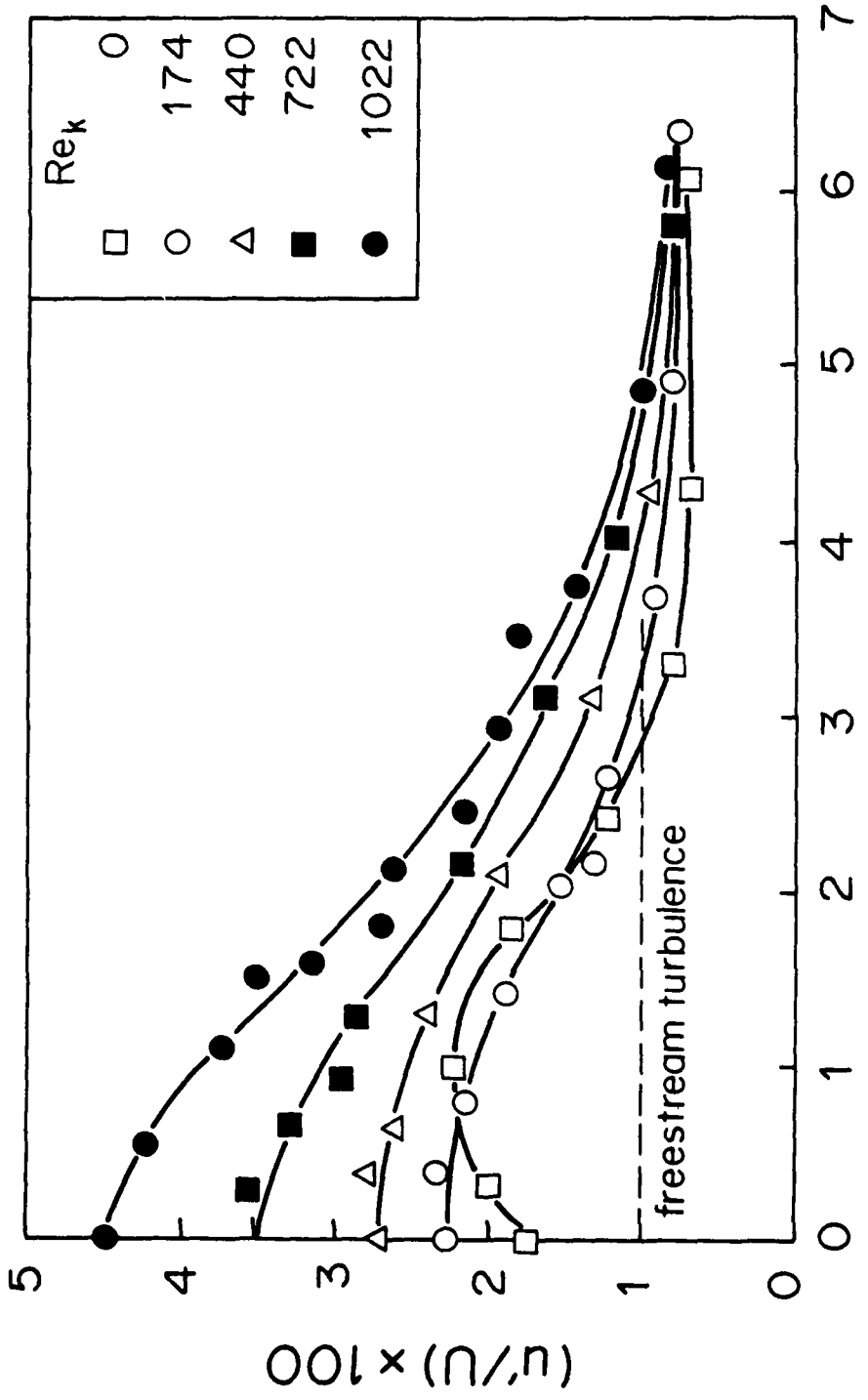

Figure 20. Wake Turbulence Intensity Profiles at X/L = 0.38

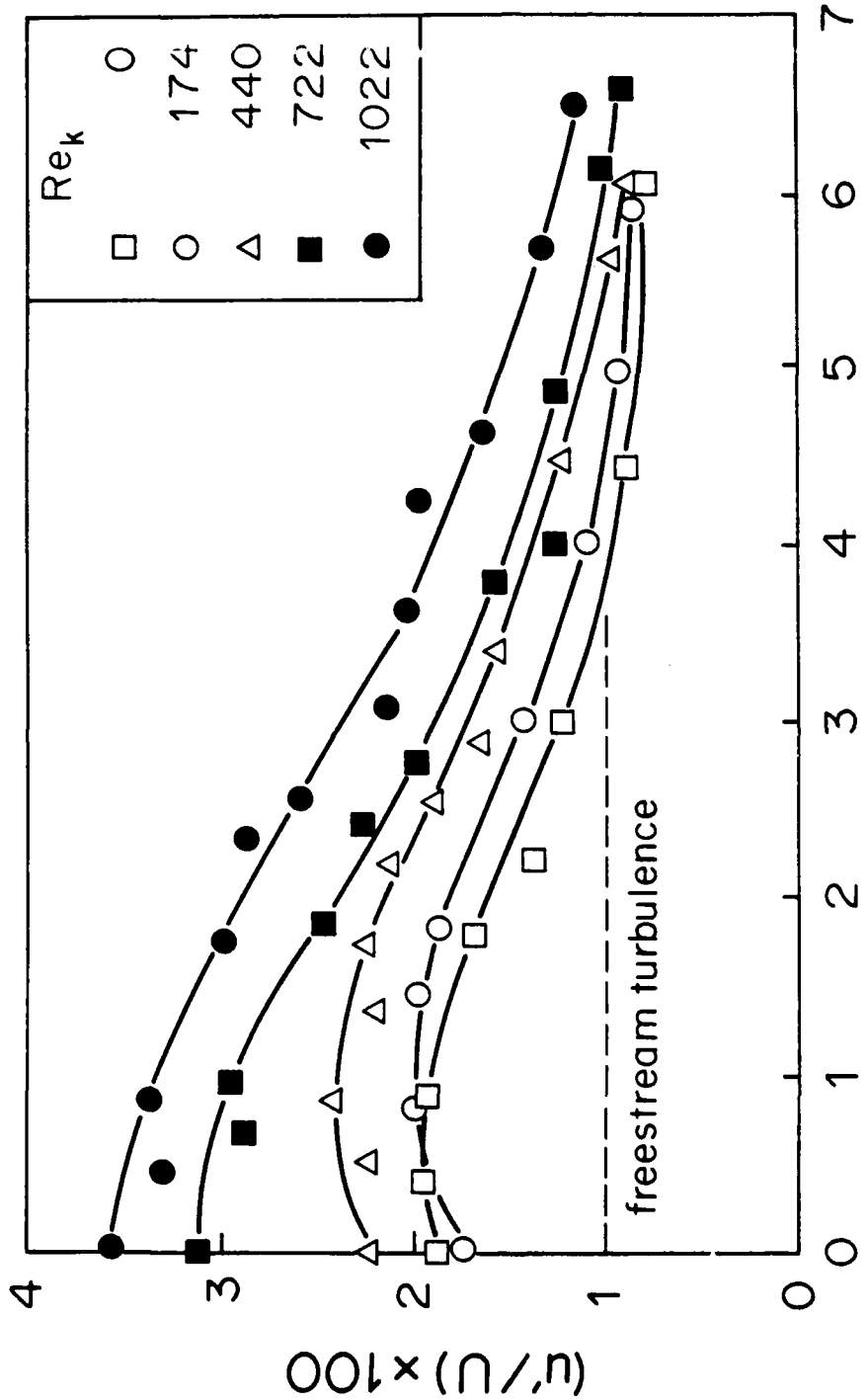

Figure 21. Wake Turbulence Intensity Profiles at X/L = 0.96

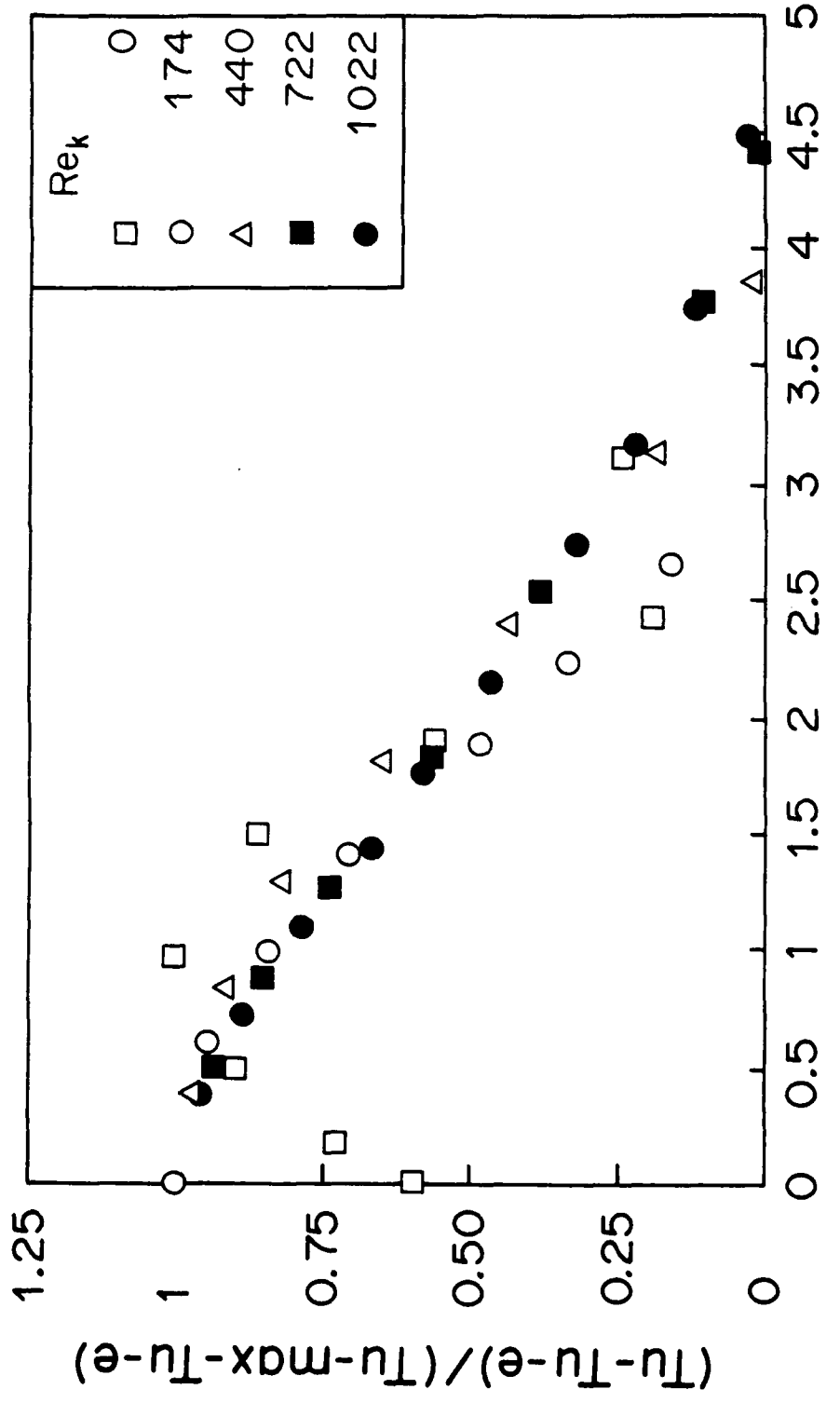

Figure 22. Normalized Turbulence Intensity Distributions

IV. HEAT TRANSFER ON ROUGH SURFACES

IV.1 The Current State of Rough-Wall Heat Transfer Analysis

The effect of wall roughness in enhancing heat transfer has long been recognized by the heat transfer community. More organized approaches have been undertaken by the energy industry in order to promote heat transfer in nuclear reactors, domestic and industrial heat exchanging devices, etc. Only in the last decade or so has the topic begun to receive increasing attention from the aerospace engineers. It has been the general conclusion that the rules of extrapolation based on empiricisms, while useful in approximate evaluation, do not yield the more refined degree of confidence needed in aerospace applications where the relative speed between a gas stream and the adjacent surface is high. For low subsonic flights or in turbine engines with low shaft speeds, the rules of extrapolation serve the needs adequately. Partly because of the low speeds, surface roughness effects are predictable within the scope of the correlation equations derived from non-aerospace sources of data. With increasing speeds, however, two factors compound one another: one is that high speeds magnify the influence of the physical size of surface roughness, as numerous investigations have shown that surface protrusions exert their fluid dynamic effects through the parameter ($k\ u_t/\nu$), where u_t is the surface shear stress. In other words, higher speeds are equivalent to larger surface roughnesses. Secondly, at higher speeds, more interacting parameters make the simpler correlation equations less likely to produce reliable results. The type of correlation equations are typified by that recommended by Norris [19], who has analyzed 13 sets of data sources and was led to a simple equation to relate heat transfer augmentation ratio with friction factor ratio due to surface roughness:

$$St/St_S = [C_f/C_{f\text{-}s}]^n, \tag{14}$$

where the exponent is dependent on the fluid Prandtl number by

$$n = 0.68\ Pr^{0.215}. \tag{15}$$

The recommended range of the friction ratio is approximately 3, beyond which the Stanton number ratio remains constant. For Pr=0.7, the author of [19] indicated that the correlation is compatible with the experimental data of Dippery and Sabersky [7]. Correlation equations such as Eq. (14) are indeed useful, especially where the streamwise variations of friction and the Stanton number are not large or remain constant—a condition certainly fulfilled in fully established duct flows. For flow configurations where streamwise variations are not insignificant, this type of correlation is not suitable because upstream "history" is important. The theoretical base in Eq. (14) can be traced back to the concept of kinetic energy of turbulence and dissipation. Indeed, such an approach was used by Kadar [13] in 1965, whose results may be expressed, for equilibrium flows, by

$$h \sim u_t. \tag{16}$$

This reduces to Eq. (14) with n=0.5 and is in reality the basic relation used by subsequent authors in formulating their rules of predicting heat transfer from friction data or analysis. Without downgrading their merits, predictive schemes based on the 1/2-power relation, such as those of Finston [10] and others, is but an expedient step. Their analysis is focused on external flows with ablation heat transfer. Similarly, the work of Dirling [8] followed the same correlation principle. Voisinet [27], in his experimental work on mass transfer over rough surfaces, confirmed the general power law relation for low mass transfer rates.

A more fundamental approach is used, however, in an investigation by Christoph and Pletcher [5], who numerically integrated boundary layer equations for flow over rough surfaces in which the mixing length is modified by Cebeci's recommendation of a normal distance shift. For the eddy thermal conductivity, however, a fixed turbulent Prandtl number is used. Bamerian and NcKillop [2] in their work had used an essentially similar approach.

Not to be overlooked are the more elaborate correlation equations developed by Kadar and Yaglom [13], who deduced a useful relation based on an extensive analysis of heat transfer data in

ducts with rough surfaces, with reactor cooling as a beneficiary. By a combination of wall-law analysis and extensive data (mainly Soviet sources), their recommended relations are:

$$Nu_d = Re_d \sqrt{C_f}/[4.3 \, Log_e \, (Re_d \sqrt{C_f}) - 2.] \tag{17}$$

for pipe flows, and

$$Nu = Re_x \sqrt{C_f}/[4.3 \, Log_e \, (Re_x \sqrt{C_f}) + 3.8] \tag{18}$$

for external flows over a flat plate.

A more fundamental—but less convenient from a engineering viewpoint—relation was given by a most recent work of Vilemas and Adomaitis [26], whose formulations are:

$$C_f = 0.021 \, Re_1^{-0.2} + 0.0032 \, [1\text{-exp} \, (-0.05 \, k^+)], \tag{19}$$

$$S_t = 0.0146 \, Re_1^{-0.24} + 0.0025 \, [1\text{-exp} \, (-0.07 \, k^+)]. \tag{20}$$

Both equations are intended for external flow applications.

Another relation, which is in reality a similarity rule, is derived by Dippery and Sabersky [7] in the form of

$$C_f/(2S_t) = 1 + [g(k^+) - 8.48] \sqrt{C_f}, \tag{21}$$

where $g(k^+)$ is a function of Prandtl number of k^+.

The function $g(k^+)$ was obtained by Dippery and Sabersky from their data of heat transfer on rough-walled circular tubes and has the following asymptotic form:

$$g(k^+) = 0.19\,(k^+)^{0.8}\,Pr^{0.44}, \tag{22}$$

for large values of k^+. For intermediate values of k^+, they are given in Fig. 23 for the Prandtl numbers of the fluids tested in their work. As Pr=0.7 is of interest to the present work, an extrapolated curve for Pr=0.7 has been added to the figure.

The previously mentioned correlation equations will be compared with the predicted results based on a finite-difference marching method developed subsequently in the present work.

On the experimental side, there is an extensive list of investigations on various aspects of flow and/or heat transfer over rough-surface boundary layers. Experimental data that can be directly linked to the surface roughness are, however, scanty. To highlight the difficulty that arises in making a direct comparison, the work of Moffat, Heazler, and Kays [16], for example, has made extensive measurements of heat transfer on a rough surface formed by tightly packed spheres. Experimental data were collected with a principal purpose to study the effect of blowing in such a configuration. Their results, though significant, are expressed in terms of the internal parameters of the flow field such as the enthalpy thickness. On a laboratory scale, quantities such as the enthaly thickness are not known a priori. And, of course, blowing makes the situation more involved. On a more fundamental level, however, there exist a number of investigations from which some basic information can be extracted to form a conceptual model to be developed in the following sections. First, a method proposed by Cebeci [3] for calculating turbulent heat transfer on smooth surfaces is discussed, followed by a review of a method proposed by Han [12] to calculate the development of turbulent boundary layers on rough surfaces. By joining these two together, and with information from other sources, an amplification factor, R, for thermal mixing length is evolved. Finally, calculations by finite-difference marching are performed for flow over a rough flat plate to obtain the Stanton numbers.

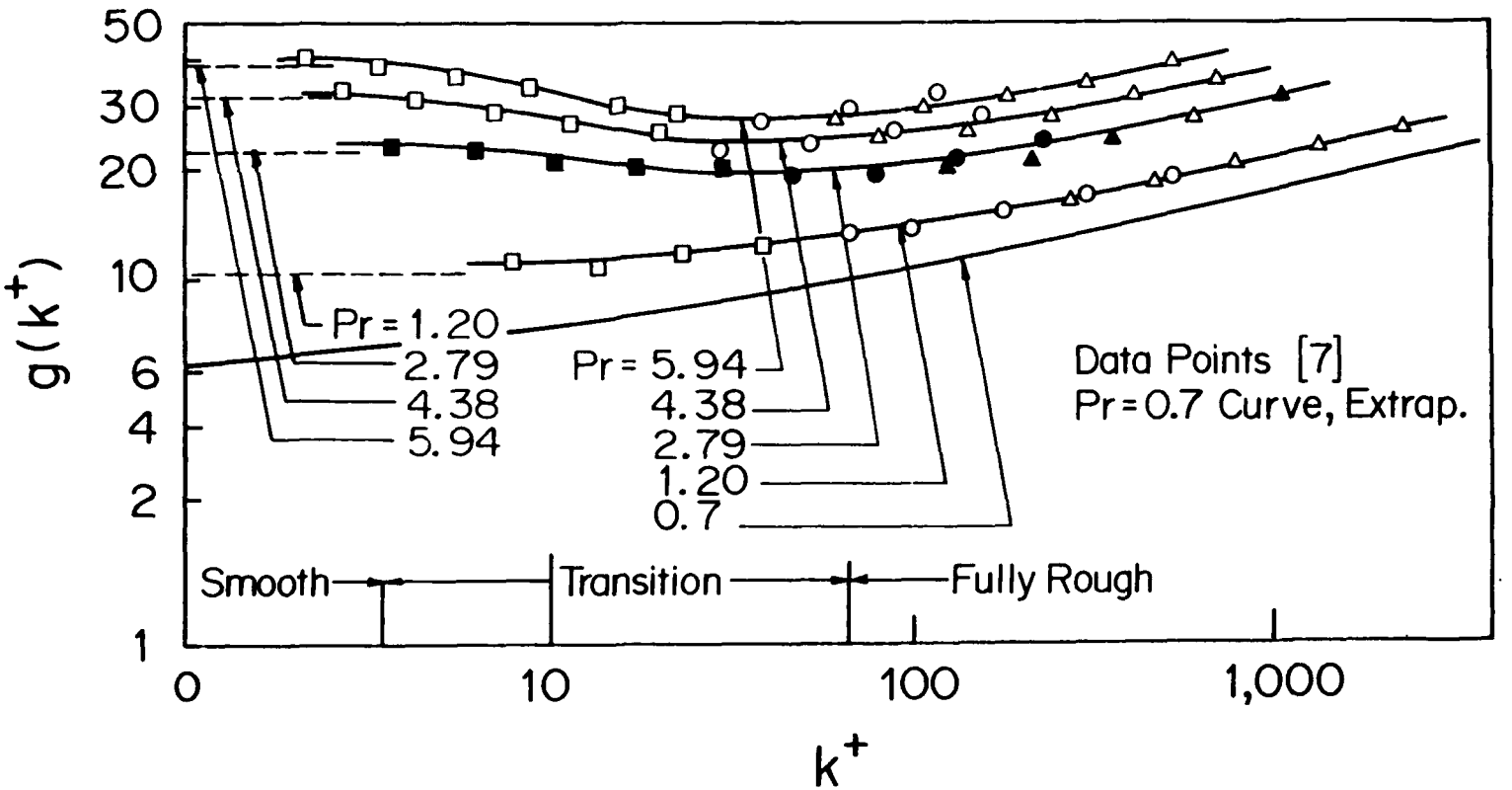

Figure 23. Dippery and Sabersky's G-function, Eq. 22

IV.2 The Thermal Mixing Length Model: Smooth Surface

With the turbulent Prandtl number, Pr_t, defined as the ratio of turbulent momentum diffusivity to turbulent eddy conductivity,

$$Pr_t = \varepsilon_m/\varepsilon_h. \tag{23}$$

Cebeci [3] showed that a model for calculating the turbulent Prandtl number,

$$Pr_t = \{K_m\,[1-\exp(-y^+/26)]\}/\{K_h\,[1-\exp(-y^+/N)]\}, \tag{24}$$

can be used in conjunction with the van Driest's modification [25] of Prandtl's mixing length in calculating heat transfer on various types of smooth-surface configurations. Pipe flows and external boundary layer flows are included. It was further specified that in Eq. (24), K_m, being the von Karman's constant, takes on the commonly accepted value of 0.4 and that 0.44 is the value for K_h, the latter being a thermal equivalent to K_m. Without the exponentials in Eq. (24), the expression reverts back to Prt=.9, a popularly used value in heat transfer analyses.

In Eq. (24), N is a parameter depending on the fluid Prandtl number and was earlier obtained by Na and Habib [18] in their analysis of heat transfer in pipe flows. The values for N recommended by Na and Habib are:

Na and Habib's N-values [18]

Pr	0.4	0.5	0.6	0.7	1.0	2.0	3.0
N	44.00	41.28	38.95	37.40	34.96	33.14	32.94

Even though their tabulated values covered a range of Pr up to 100, such a wide span is not needed in this work.

To summarize, Cebeci's method consists in first calculating a mixing length, then the momentum eddy diffusivity, and finally the thermal eddy diffusivity by the following equations in dimensionless notations:

$$\ell^+_m = K_m\, y^+ \,[1-\exp\,(-y^+/26)], \tag{25}$$

$$\varepsilon^+_m = (\ell^+_m)^2\,[du^+/dy^+], \tag{26}$$

$$\varepsilon^+_m = \{K_m y^+\,[1-\exp\,(-y^+/26)]\}^2\,(du^+/dy^+), \tag{27}$$

$$\varepsilon^+_h = [K_m y^+][K_h y^+][1-\exp\,(-y^+/26)][1-\exp\,(-y^+/N)]. \tag{28}$$

The turbulent viscosity obtained from Eq. (27) is limited to the maximum value (Clauser) given by

$$\varepsilon^+_m = 0.0168\ Re_1 \tag{29}$$

and is further modified by an intermittency factor of

$$F = 1/[1+5.5\,(y/\delta)^6], \tag{30}$$

where: Re_1 = displacement thickness Reynolds number

δ = boundary layer thickness defined as where the velocity of 0.99 of the free stream.

In the case of the thermal eddy diffusivity ε^+_h of Eq. (28), not enough is known about its appropriate upper limit. However, by an extension of the Reynolds analogy, the same upper

bound as given by Eq. (29) is used here, as is elsewhere. And, of course, the intermittency function F in Eq. (30) is also part of the boundary layer analysis model.

The preceding set of equations due to Cebeci [3] represents the only existing physical model suitable for finite difference computation of the flow and temperature fields.

The turbulent Prandtl number in Eq. (24) varies in the space coordinate y^+, as contrasted with a fixed turbulent Prandtl number of 0.9 across the entire boundary layer—a commonly used procedure. The validity of Eq. (24) has been substantiated by Cebeci [3] for flows over smooth surfaces. In addition, turbulent Prandtl number data from measurements by Simpson [23] compared favorably with the calculated distributions from Eq. (24). Furthermore, from the viewpoint of end results, the calculated heat transfer data for pipe flows are in good agreement with measurements. Despite these favorable observations, the question remains as to how to extend Eq. (24) to rough-wall heat transfer analysis. This is taken up next.

IV.3 The Thermal Mixing Length Model: Rough Surfaces

It has been shown in [12] that the Cebeci-Smith model with mixing length given by the usual van Driest's formula can only be extended to rough surfaces analysis by introducing an additive mixing length in the van Driest's damping formula. Also in [12], an alternative with no loss of accuracy is to use an exponential expression, Eq. (5), for the mixing length. With this form, it is then possible to account for the wall roughness by an amplication factor, R_m, as a multiplier to Eq. (5), thus resulting in a wall-law velocity profile with a downshift of the dimensionless velocity, u^+. This is a common element of the exponential model to be developed. Hence for smooth surfaces, i.e., $R_m=1$, Eqs. (5) and (25) are not different from each other, as has been demonstrated before. With Eq. (5) multiplied by R_m as a basic modification, there evolve two candidate mathematical forms of thermal models:

(i) The first model for the thermal mixing length for rough surfaces is the replacement of Eq. (25) by Eq. (5). In the momentum mixing length expression, Eq. (5), an amplification factor, R_m, for surface roughness effect is used as a multiplier, resulting in increased turbulence.

The entire assembly of equations therefore consists of Eqs. (5), (26), (31), and (32). For clarity, they are grouped together:

$$\ell^+_m = R_m\,(K_m/E_m)[\exp\,(K_m u^+) - \exp\,(-K_m u^+)], \tag{5}$$

$$\varepsilon^+_m = (\ell^+_m)^2\,[du^+/dy^+], \tag{26}$$

$$\varepsilon^+_m = \{R_m\,(K_m/E_m)[\exp\,(K_m u^+) - \exp\,(-K_m u^+)]\}^2\,[du^+/dy^+], \tag{31}$$

$$\varepsilon^+_h = \varepsilon^+_m/Pr_t, \tag{32}$$

where Pr_t is that defined by Eq. (24).

The first test of this model is, of course, whether the wall law thermal profile obtained by setting R_m=1 in Eq. (5) in the preceding set is in agreement with that from Cebeci's thermal model described in the previous section. This shall be done in the final evaluation.

(ii) A second for the thermal eddy conductivity departs from the preceding one in that a thermal mixing length is defined in an exponential form dependent on T^+, instead of u^+. The resulting expression for the turbulent eddy conductivity is the product of the momentum mixing length, thermal mixing length, and the local normal gradient of the velocity. The momentum mixing length is that defined by Eq. (5). The thermal mixing length model is developed as follows:

By defining a nondimensional temperature in the wall-coordinates as

$$T^+ = \rho c u_t [T-T_w]/q, \tag{33}$$

the thermal mixing length is proposed to be

$$\ell^+_h = R_h (K_h/E_h)[\exp(K_h T^+) - \exp(-K_h T^+)], \tag{34}$$

where R_h is the thermal mixing length amplification due to surface roughness. In this model, the eddy conductivity is embedded in the following:

$$\varepsilon^+_h = (\ell^+_m)(\ell^+_h)[du^+/dy^+], \tag{35}$$

in which ℓ^+_m is that of Eq. (5) and ℓ^+_h that of Eq. (34). The complete form for ε^+_h is then

$$\varepsilon^+_h = \{R_m (K_m/E_m)[\exp(K_m u^+) - \exp(-K_m u^+)]\}$$

$$\{R_h (K_h/E_h)[\exp(K_h T^+) - \exp(-K_h T^+)]\} (du^+/dy^+). \tag{35a}$$

Note that in the second model, the turbulent Prandtl number defined by Eq (24) is bypassed. Of course, the auxiliary equations (29) and (30) still apply in this model.

The principal features in this model are, in addition to the thermal mixing length amplification, R_h, the thermal wall-law slope, K_h, and the thermal wall-law intercept E_h. Although E_h and R_h appear in a product, each is dependent on separate parameters. In the case of E_h, it is governed by the fluid Prandtl number, and in the case of R_h by the roughness parameter, k^+. Their variations with their respective parameters are to be determined separately.

Beginning with smooth surface for which thermal profiles in the boundary layers have been measured or calculated to the extent that heat transfer results were in good agreement with data, the task begins by setting R_h at 1, i.e., for smooth surface, with the sole purpose of establishing how

E_h varies with Pr. To this end, it is first recalled that a Couette flow analysis (constant shear) implies the following heat transfer relation,

$$[(1/Pr) + \varepsilon_h^+] \, (dT^+/dy^+) = 1. \tag{36}$$

In the asymptotic region with large values of y^+, ε_h^+ dominates the first term and is effectively the first term of Eq. (34) for ℓ_h^+. Thus, the result of integration yields the wall-law for T^+ as,

$$T^+ = (1/K_h) \, Log_e \, (y^+) + C_h \tag{37}$$

and the corresponding equation for u+ of which Eq. (1) is a special case becomes

$$u^+ = (1/K_m) \, Log_e \, (y^+) + C_m. \tag{38}$$

Some investigators [15] prefer another form:

$$T^+ = Pr_t \, [(1/K_m) \, Log_e \, (y^+) + C_{th}], \tag{39}$$

which is a variant of Eq. (37). By comparing terms, it follows that

$$Pr_t = K_m/K_h \qquad \text{and} \qquad C_h = Pr_t \, C_{th}.$$

The integration constant C_h and C_m are related to E_h in Eq. (34) and to E_m in Eq. (5) by the following:

$$E_m = \exp \, (K_m C_m), \tag{40}$$

$$E_h = \exp(K_h C_h). \tag{41}$$

Having established the connection between C_h and E_h, the next step is to determine how E_h varies with the fluid Prandtl number. First, the question of what K_h value to use is to be settled. The thermal wall-law slope K_h has a number of variances. There are at least three sources which give the thermal wall-laws that use slightly different values for K_h and the thermal law intercept constant C_h. Each pair of C_h and K_h for a fixed Prandtl number results in a value for E_h. The following shows their variances for Pr=0.72 (air):

K_h	C_h	E_h	Source
0.44	4.363	6.82	Cebeci [3]
0.456	3.375	5.482	Kays et al. [14]
0.47	4.340	7.690	Kadar et al. [13]

Of the three sets of numbers, Cebeci's is based on a physical model (K_m=0.4) that results in heat transfer in good agreement with data. For this reason, the values of Cebeci's recommendation data for Pr=0.72 were taken. His value for C_h was obtained by using Eq. (28) with an appropriate value for N from Na and Habib's tabulation. Eq. (28) was put into Eq. (36) to calculate a thermal profile of T^+ from y^+=0 to where the thermal wall-law can be recognized at which C_h can be determined. Thus, there exists a value of E_h for each Prandtl number. This procedure just described produced a list of E_h's for Prandtl numbers from 0.72 to 5.7 shown below:

E_h vs. Pr-variation with N, from [18]

Pr	0.72	1.	3.	5.7
E_h	6.82	21.5	0.21×10^5	0.827×10^7

With E_h—intended for Eq. (34)—extracted from Cebeci's smooth model, thus ensuring that their respective wall-laws for T^+ would coincide, it is of interest to examine their profiles in the buffer region. Integration of Eq. (36) for the two models for ε_h^+, i.e.. Eq. (28) and Eq (35a), produces various distributions for Pr from 0.72 to 5.7. For low values, these two methods give almost identical profiles shown in Figure 24. Since the present work is concerned with gas flows, i.e., Pr=0.7, discrepancies at larger Prandtl numbers are not a major concern.

IV.4 The Thermal Mixing Length Amplification, R_h.

There are two ways to quantify the thermal amplification R_h. One is to compare heat transfer data on smooth surfaces and that on surfaces whose roughnesses have been characterized. Heat transfer predictions are then made, based on the eddy conductivity model of Eq. (35a) with an amplification factor R_h so determined that the predicted heat transfer is in accord with measured data. The method is an ideal but tedious approach, not to mention the lack of heat transfer data meeting the stated criteria. A second way is to rely on a few of measured temperature profiles in rough-wall boundary layers. From the data, R_h can be calculated.

Ideally speaking, both methods should agree; but, in reality, it will hardly be the case. It is the second approach that is used in the present work. The model so constructed will be checked by reference to a few data bases for which the surfaces can be quantitatively characterized.

Review of the Momentum Amplification, R_m

Since the development of R_h parallels that of R_m, the momentum amplification, it is pertinent to retrace a few steps for the latter to lead into the development of the thermal amplification.

In the wall-law region, the velocity distribution for a rough surface is found to follow

$$u^+ = (1/K_m)\,\mathrm{Log}_e\, y^+ + C - \Delta u^+ \qquad (42)$$

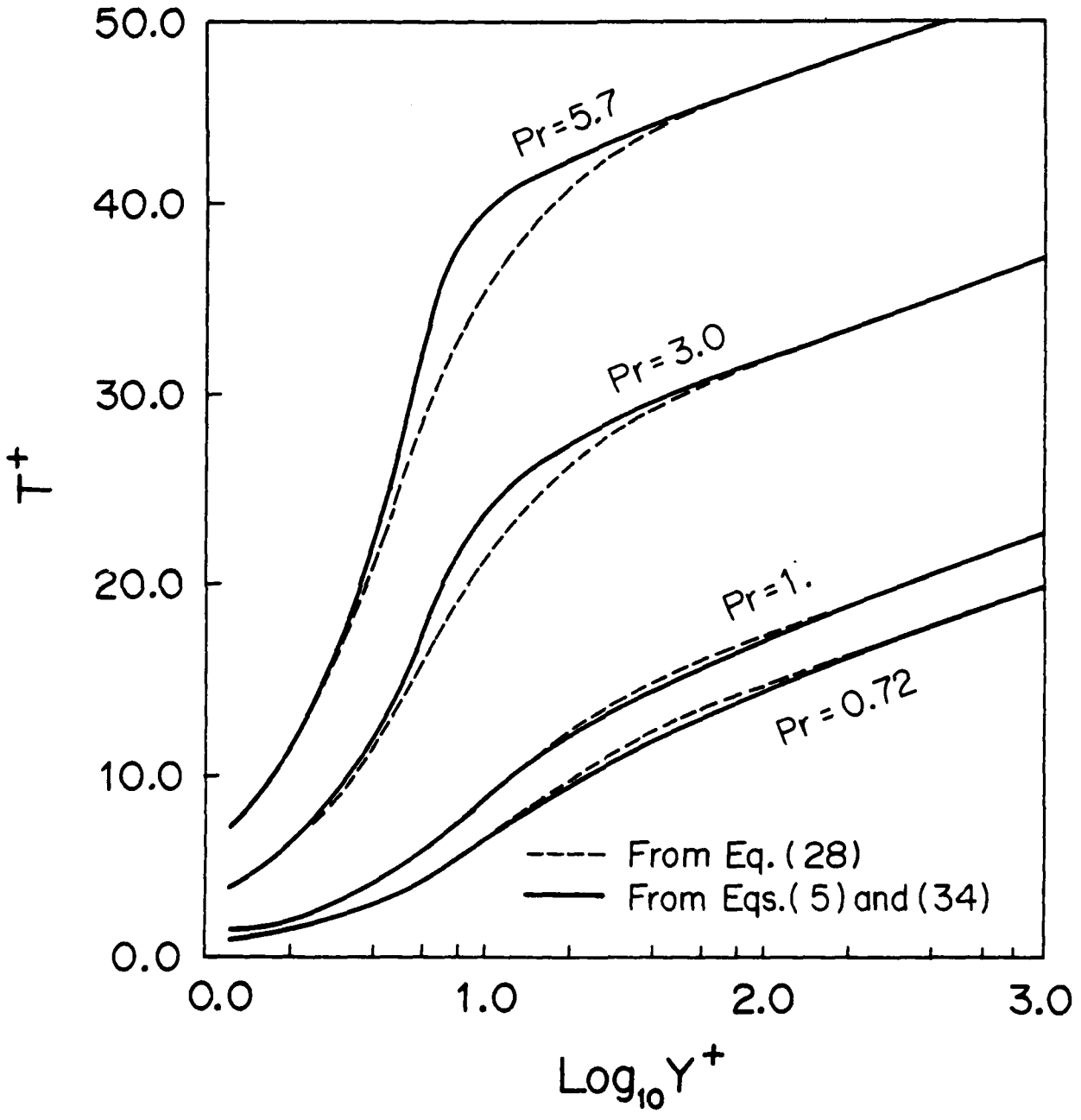

Figure 24. Comparative Temperature Profiles for Smooth Surface.

which differs from Eq (38) in the Δu^+-term only. Nikuradse used, however, a function, B_m, which varies with k^+, as follows

$$u^+ = (1/K_m)\,[\mathrm{Log}_e\, y^+ - \mathrm{Log}_e\, k^+] + B_m \tag{43}$$

Connecting the equations (42) and (43), Δu^+ is related to B_m by

$$B_m = C_m + (1/K_m)\,\mathrm{Log}_e\, k^+ - \Delta u^+. \tag{44}$$

For small values of k^+, Δu^+ vanishes. Hence the functional dependence of B_m on k^+ is of the form

$$B_m = C_m + (1/K_m)\,\mathrm{Log}_e\, k^+ \tag{45}$$

as k^+ approaches zero. Nikuradse's data for a wide range of sandgrain roughnesses confirmed the trend in Eq. (45) and established a plateau value of 8.48 for k^+ greater than 90.

Using the exponential model for the momentum mixing length, Eq. (5a), the resulting wall-law can be put as

$$u^+ = (1/K_m)\,[\mathrm{Log}_e\, y^+ + \mathrm{Log}_e\, E_m - \mathrm{Log}_e\, R_m]. \tag{46}$$

Its comparison with Eq. (4) establishes the relations between Δu^+, R_m, and B_m:

$$\Delta u^+ = (1/K_m)\,\mathrm{Log}_e\, R_m \tag{47}$$

$$R_m = k^+ \exp\,[K_m\,(C_m - B_m)] \tag{48}$$

At large values of k^+, B_m is 8.4 and Eq. (48) becomes a linear relation between R_m and k^+, with a slope of β_m as indicated in Eq. (7). Values of R for Nikuradse's sandgrain roughness as well as three other types of roughnesses—Hama's wirescreens, Moody's random, and Cole-Brook-White mixed sandgrain—have been determined and reported in an earlier work [12].

Analogous to Nikuradse's roughness data, Ligrani and Moffat [15] have performed measurements of the temperature profiles over rough surfaces formed by tightly packed spheres. Their treatment of the data is as follows: First, Eq. (39) is extended to include two roughness effects. One is a temperature gap between the roughness elements and the fluid in the immediate vicinity of the surface protrusions and the other is a spatial-dependent temperature shift. It is the latter temperature shift that increases heat transfer over rough surfaces. Eq. (39) thus extended becomes

$$T^+ = Pr_t [(1/K_m) \text{Log}_e y^+ + C_{th}] - \Delta T^+ + \delta T^+, \tag{49}$$

where ΔT^+ is the spatially dependent temperature shift and δT^+ is the surface temperature gap, whose magnitude is given by Dippery and Sabersky [7] as

$$\delta T^+ = \phi Pr^{0.4} (k^+)^{0.2} \tag{50}$$

It must be mentioned that δT^+, as demonstrated to be a temperature gap in the near vicinity of surface roughness elements, is not part of the model considered. Its role in affecting heat transfer predictions is greatly outweighed by the uncertainty of the predictive process itself, though its significance in experimental work only begins to be recognized. Another significant experimental finding in rough-wall boundary layers is the correct origin for reckoning y in order to establish wall-law plots; it was found to be about 0.7 of the roughness height from the bottom, according to Voisinet [27] and Perry and Joubert [20].

Similar to the B_m-function defined by Nikuradse, a corresponding function for the temperature shift ΔT^+ is defined by

$$T^+ = Pr_t\,[1/K_m)\,(Log_e\,y^+ - Log_e\,k^+) + B_{th}] + \delta T^+ \qquad (51)$$

which, when connected with Eq. (49), provides a link between B_{th} and ΔT^+ in the form of

$$\Delta T^+ = Pr_t\,[C_{th} + (1/K_m)\,Log_e\,k^+ - B_{th}]. \qquad (52)$$

Values of B_{th} at various roughness Reynolds numbers k^+ were measured by Ligrani and Moffat [15] on the sphere-formed surface. In their evaluation of B_{th}, Pr_t is set at 0.9 and C_{th} at 4.15, consistent with the correlation by Kays and Crawford [14]. Three distinct regions of B_{th} exist: one for k^+ greater than 55, the fully turbulent region in which B_{th} equals 8.48, the same asymptote for Nikuradse's B_m; one for k^+ less than 2.25, the hydraulically smooth region in which B_{th} is such that $\Delta T^+ = 0$; and one between the two limits, the transitionally rough region in which different types of roughnesses exert their individual characteristics. For the sphere-roughened surface, Ligrani and Moffat's data can be represented, according to these authors' recommendation, by the following:

Expressing the lower and upper demarcation values for k^+ as k^+_1 and k^+_2, which in the case of sphere-roughened surfaces are 2.25, and 55 respectively, and using the functional notation, W,

$$W = C_{th} + (1/K_m)\,Log_e\,k^+, \qquad (53)$$

the function B_{th} can be separately represented by three segments given by the following:

(i) Hydraulically Smooth Region, k^+ less than k^+_1,

$$B_{th} = W \tag{54a}$$

(ii) Transitional Region—k^+ greater than k_1^+ but less than k_2^+,

$$B_{th} = W - (W - 8.48) \sin(\phi\pi/2) \tag{54b}$$

(iii) Fully Rough Region—k^+ greater than k_2^+

$$B_{th} = 8.48 \tag{54c}$$

The function ϕ is a linear interpolation of the Log of k^+ between k_1^+ and k_2^+, i.e.,

$$\phi = [\text{Log}(k^+) - \text{Log}(k_1^+)]/[\text{Log}(k_2^+) - \text{Log}(k^+_1)] \tag{55}$$

The Link Between B_{th} and R_h

The discussion up to this point has led to the establishment of B_{th} for an input value of k^+. The final step is to relate B_{th} with R_h needed to complete the thermal mixing length of the second model. Since the eddy conductivity is modeled by Eq. (35a) and its asymptotic behavior at large y^+ is the same as the thermal mixing length in Eq. (34), use of the later in Eq. (36) results in a thermal wall-law given by

$$T^+ = (1/K_h)\,\text{Log}_e\, y^+ + C_h - (1/K_h)\,\text{Log}_e\, R_h \tag{56}$$

wherein $C_h = (1/K_h)\,\text{Log}_e\, E_h$. By comparing Eq. (56) with the case of R_h=1, i.e., Eq. (37), the temperature shift ΔT^+ is therefore given by

$$\Delta T^+ = (1/K_h)\,\text{Log}_e\, R_h \tag{57}$$

$$R_h = (k^+) \exp [K_m (C_{th} - B_{th})]. \quad (58)$$

There are two sets of numerical constants for air (Pr=0.7) in the literature. Ligrani's values and their associated parameters in the exponential model are:

$C_m = 5.10$	$K_m = 0.41$	$Pr_t = 0.9$	$K_h = 0.456$
$C_h = 3.74$	$C_{th} = 4.15$	$E_h = 5.482$	

and another set of values from Cebeci [3] are:

$C_m = 5.5$	$K_m = 0.40$	$Pr_t = 0.9$	$K_h = 0.44$
$C_h = 4.36$	$C_{th} = 4.85$	$E_h = 6.820$	

With the B_{th}-values defined by Eqs. (53) through (55), the thermal amplification factor is computed for a range of k^+. At large values of k^+, B_{th} approaches 8.48, as does B_m, and Eq. (58) becomes a linear relation expressed by

$$R_h = \beta_h k^+ \quad (59)$$

This equation is a companion to Eq. (7) for R_m. The slopes β_h are 0.1680 and 0.1620 respectively for the two sets of constants used; despite their substantial differences, the resulting slopes are not much different. The values of R_h thus deduced from the measured thermal boundary layer profiles are tabulated in Table 1 and plotted in Figure 25 with their values close together. We should note, however, that Ligrani's data are for surfaces formed by packed spheres and for Pr=0.7. The difference in the surface textures is most likely unimportant, except in the

TABLE 1

Thermal Mixing Length Amplification Factor: Pr = 0.7
(For Sphere-Roughness)

k^+	R_h (i)	R_h (ii)
0	1	1
1	1.001	1.001
4	1.025	1.023
6	1.029	1.073
8	1.183	1.168
10	1.361	1.331
15	1.951	1.900
20	2.643	2.567
25	3.411	3.306
30	4.237	4.101
40	6.007	5.803
50	7.863	7.589
60	9.743	9.397
80	13.400	12.919
90	15.124	14.580
Slope	**0.168**	**0.162**

(i) Parametric Constants From Ref [15]
(ii) Parametric Constants From Ref [3]

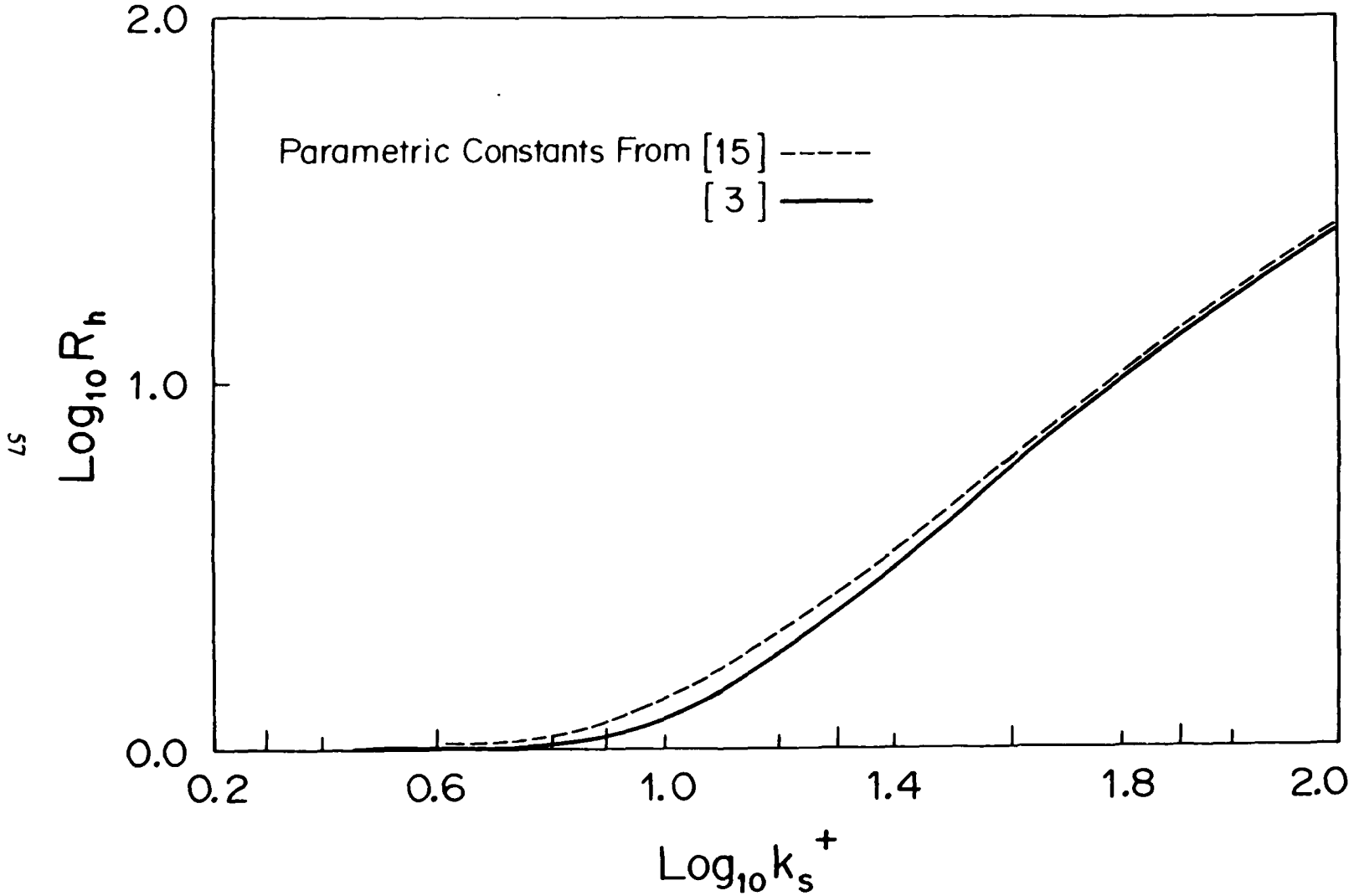

Figure 25. Thermal Mixing Length Amplification for Sphere-Roughness, Pr = 0.7

transitionally rough region with k^+ between 2.25 and 55; how influential the uncertainty is in affecting the computed results is difficult to assess.

IV.5 Calculated Heat Transfer in Boundary Layer Flows

The differences between the two rough-surface eddy conductivity models are marked by the feature that in Model-1, the eddy conductivity is independent of the temperature, while in Model-2, it is an exponential form of the local temperature. In numerical computation, the first model will admit an implicit marching algorithm while the second model requires an explicit marching scheme in which the eddy conductivity profile is computed using that of a previous station in the marching direction.

Unlike momentum boundary layer analysis, that of thermal boundary has less experience to draw on. Questions such as what limiting eddy conductivity should be imposed in the outer layer are not answerable as yet. Much needs to be explored. Here the aim is to demonstrate that the models advanced do give results that are in accord with the limited data on surfaces with roughnesses well characterized.

To test the thermal models developed for rough-wall analysis in this work, a simple marching code was developed for flat-plate boundary layers. For K_m, the von Karman's constant, 0.4 is used; and for K_h 0.44 is used. In the turbulent Prandtl expression of Cebeci, the constant N was taken as 37.15 for Pr=0.72, recommended by Na and Habib. In Eq. (35a), E_h is set to 6.82, as mentioned previously. All together, five surface roughnesses were analyzed; they ranged from 0 to 2000 for Re_k. Calculations started from the leading edge where flow is assumed turbulent. The calculated heat transfer is shown in Figure 26. The computed Stanton numbers are indicated by dashed lines for results based on Cebeci's turbulent Prandtl number modification of the eddy viscosity, and by solid lines based on the exponential model, in which a heat transfer amplification factor is used. Calculated results show practically identical augmentations using either one of the two models. Also shown is the simpler relation for smooth surfaces [22]. It is comparable to the

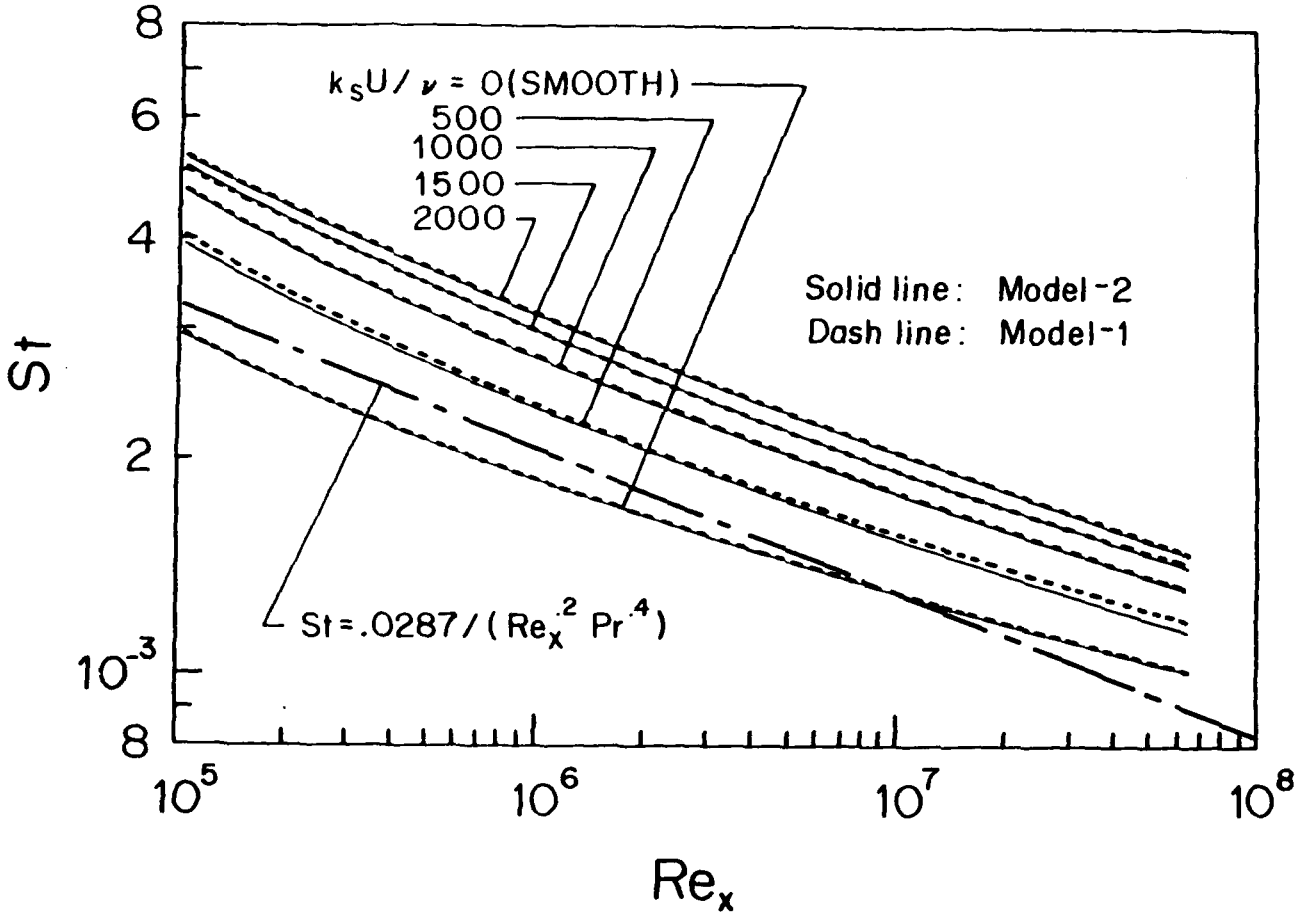

Figure 26. Heat Transfer From Flat Plate With Surface Roughness.

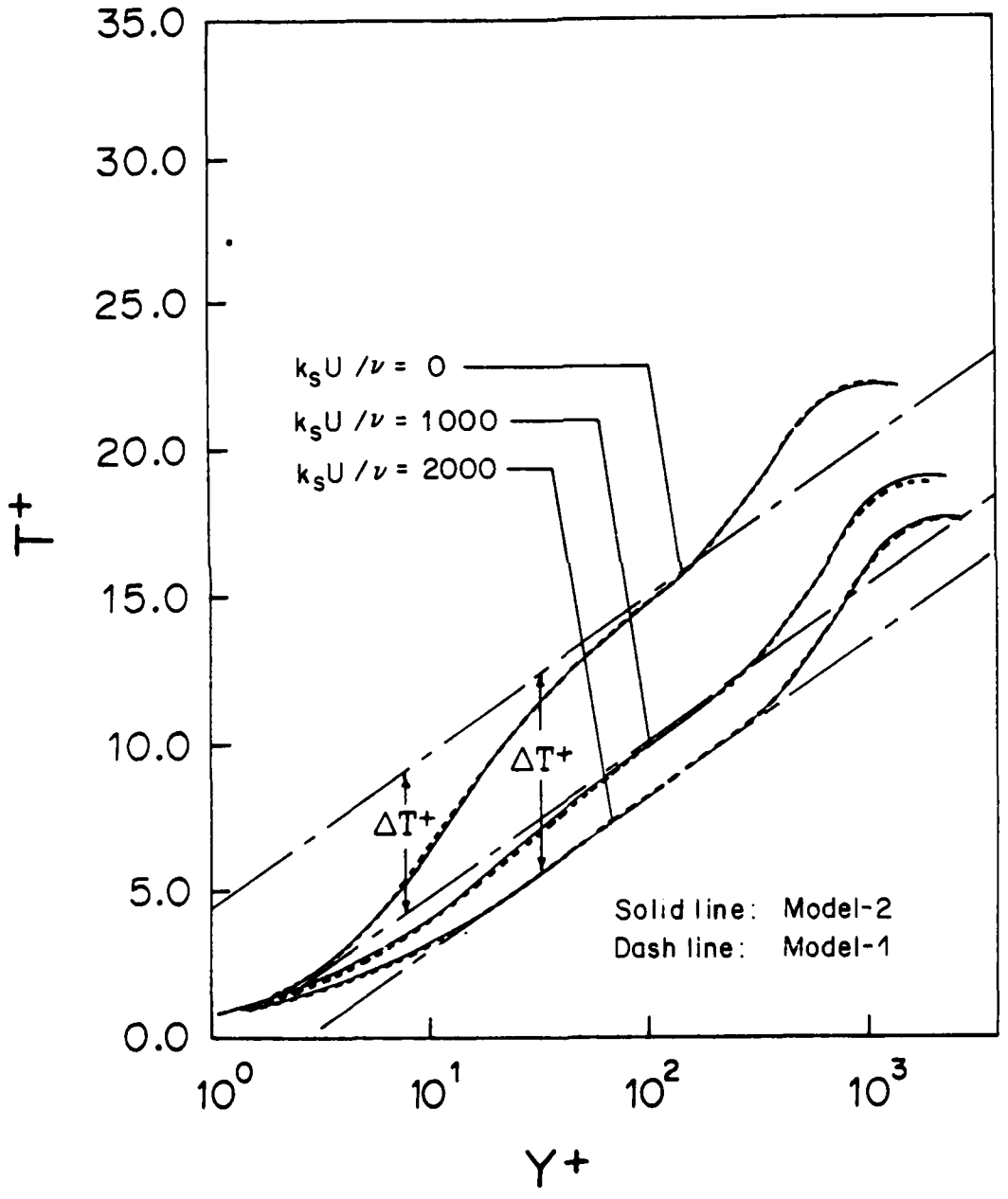

Figure 27. Temperature Profiles in Boundary Layers, $Re_x = 10^6$

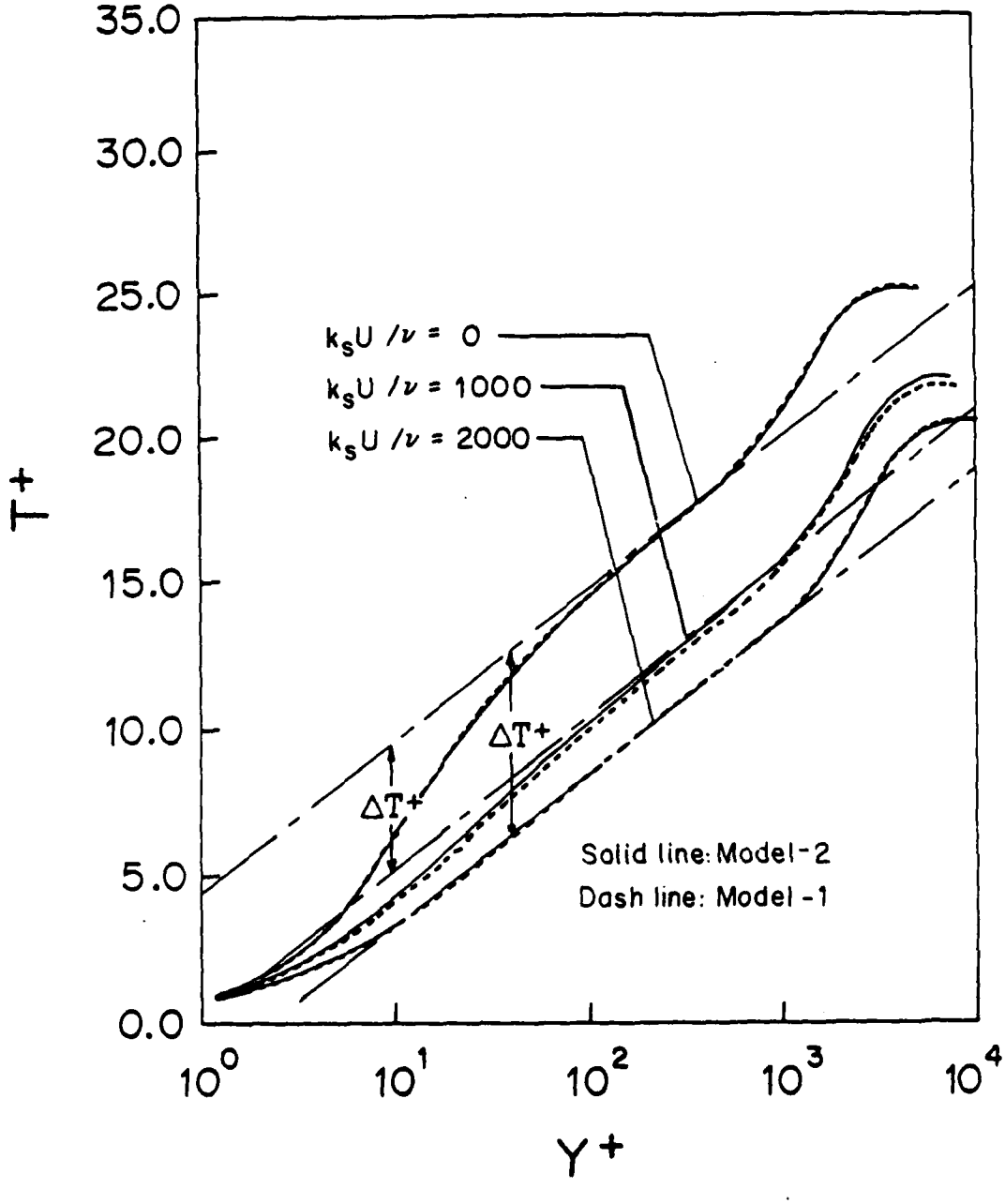

Figure 28. Temperature Profiles in Boundary Layers, $Re_x = 5.10^6$

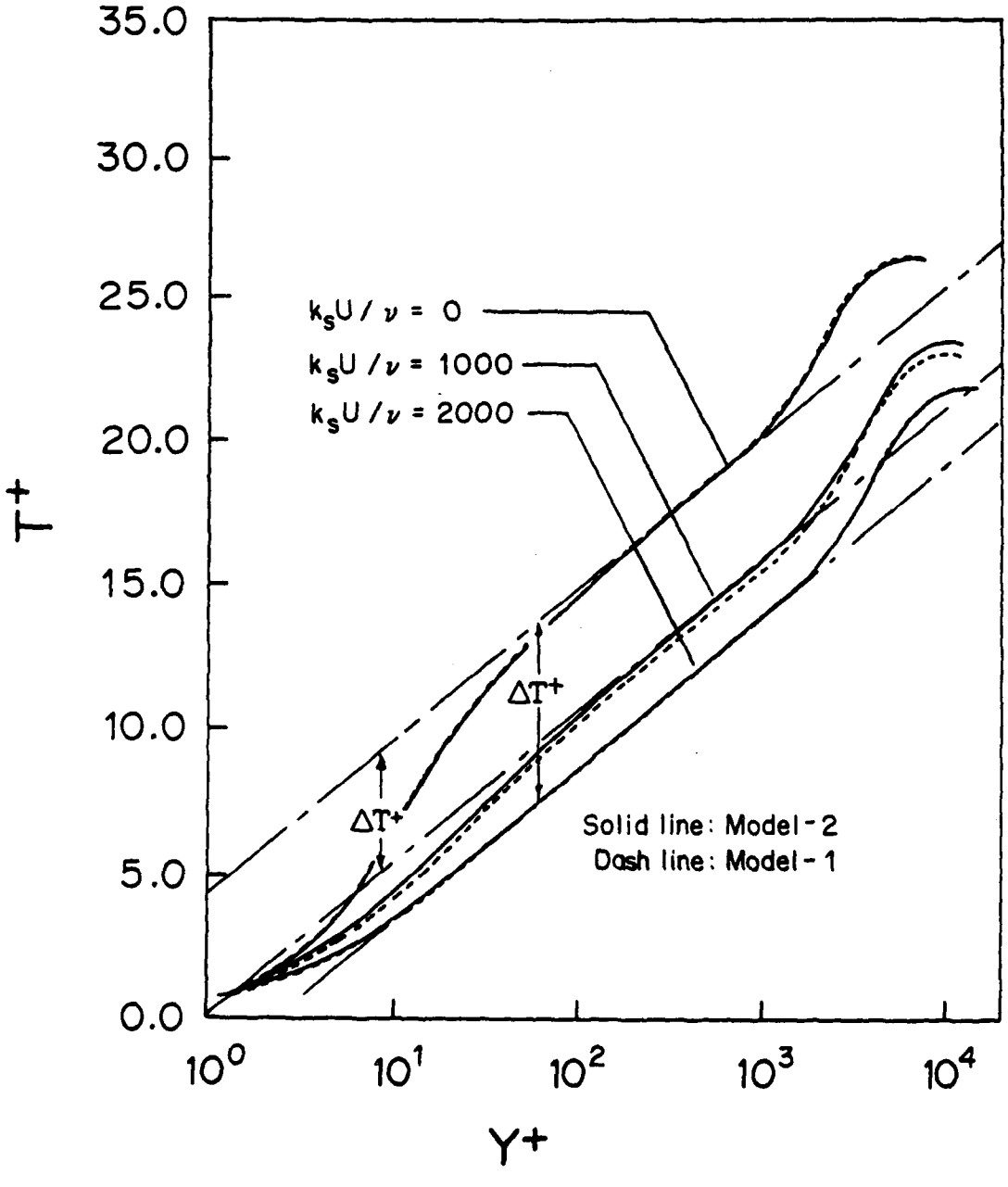

Figure 29. Temperature Profiles in Boundary Layers, $Re_x = 10^7$

predictions of the present analysis. It is, of course, understood that the simple correlation equation shown is to demonstrate their magnitudes.

To further delineate the surface roughness influence on the boundary layers, computed temperature profiles in the plus coordinates are shown in Figures 27, 28, and 29 for local Reynolds numbers of 10^6, $5 \cdot 10^6$, and 10^7. In each figure, there are three sets of curves for three roughness parameters, Re_k, equal to 0, 1000, and 2000. The roughness parameter Re_k describes the absolute roughness protrusion. Since surface roughness exerts its influence through a roughness Reynolds number, k^+, which is comprised of the surface roughness and the corresponding friction velocity, it is its numerical value that determines the downshift of the dimensionless temperature in the wall-law region. The numerical values of the roughness Reynolds numbers and other parameters of interest for Figures 27, 28, and 29 are listed in Table 2.

A point to be noted in Figure 26 is that in the leading edge region where the local shear stress is high, moderate surface protrusions are magnified through the influence of k^+ to the extent that small roughnesses in combination with large stresses produce significant heat transfer augmentations—thus demonstrating the importance of magnification. In fact, in the lower local-Reynolds-number region, a small roughness brings its effects into the fully rough region. This explains the trend in Figure 26 that different curves for different values of Re_k are, relatively speaking, closer together in the leading edge portion than in the downstream region of low shear stresses.

IV.6 Comparison with Correlations and Similarity Laws

Results were compared with those based on Eq. (20) due to Vilemas and Adomaitis [26], Eq. (18) from Kadar and Yaglom [13], and Eq. (21) obtained from Dippery and Sabersky [7]. These equations are, strictly speaking, not predictive but correlation formulas, for they require input parameters that are internal to the resulting flows: the required values for flows over rough surfaces are a local friction coefficient C_f in Eq. (18), a displacement thickness δ_1 and a roughness Reynolds number k^+ in Eq. (18), and C_f and k^+ in Eq. (21). These internal values are, of course,

TABLE 2

Computed Parametric Values, Figures 27, 28, and 29

$(k_s U/\nu)$	0	1000	2000
Figure 27 $Re_x = 10^6$	$R_m = 1.$	15.93	33.75
	$\Delta u^+ = 0.0$	6.92	8.80
	$R_h = 1.$	8.361	19.90
	$\Delta T^+ = 0.0$	4.83	6.68
	$u_t/U = 0.0415$	0.0526	0.0562
Figure 28 $Re_x = 5.10^6$	$R_m = 1.$	13.48	28.99
	$\Delta u^+ = 0.0$	6.50	8.42
	$R_h = 1.$	6.886	16.08
	$\Delta T^+ = 0.0$	4.39	6.31
	$u_t/U = 0.0365$	0.0448	0.0479
Figure 29 $Re_x = 10^7$	$R_m = 1.$	12.53	27.04
	$\Delta u^+ = 0.0$	6.32	8.24
	$R_h = 1.$	6.362	15.05
	$\Delta T^+ = 0.0$	4.21	6.16
	$u_t/U = 0.0347$	0.0419	0.0447

not known in advance, hence they only serve the purpose of comparing with the heat transfer data calculated by the present self-contained model.

Hence, the necessary input values are calculated from the rough-surface momentum model [12] to obtain C_f, k^+ for use in the correlation equations. Results of comparison generally indicate that Dippery and Sabersky's Eq. (21) in which the g-function was extrapolated to Pr=0.7 shows best overall correspondence with the present model calculations. This is shown in Figure 30, for three roughness conditions: Re_k equal to 0 (smooth), 500 and 1000. In computing Stanton numbers from Eq. (21), values for the friction coefficient, C_f, were obtained from the model based on the momentum amplification factor developed in [12] and, for the conditions of the comparison, are shown in Figure 31, which also shows an accepted empirical equation for smooth surface (dash line). The Stanton numbers in Figure 30 indicate fair agreement between the two sources, with the curves for Re_k = 500 almost indistinguishable from each other.

Turning to the two other equations, the Stanton numbers obtained from Eqs. (18) and (20) are grouped together for Re_k = 500 in Figure 32. In addition, the power law of Eq. (14) with n=1/2 is also included. A wide range of the calculated values is apparent. It cannot escape the conclusion that heat transfer relations, such as Eqs. (18) and (20), that are derived from pipe flow data over a wide range of surface roughness patterns, are not conducive to their confident applications where localized streamwise distributions are needed. On the other hand, the correlation equation due to Dippery and Sabersky, Eq. (21), though having its data base similar to those of Eqs. (18) and (20), was reached by processing the data to the level of the rough surface activities and is hence comparatively more creditable.

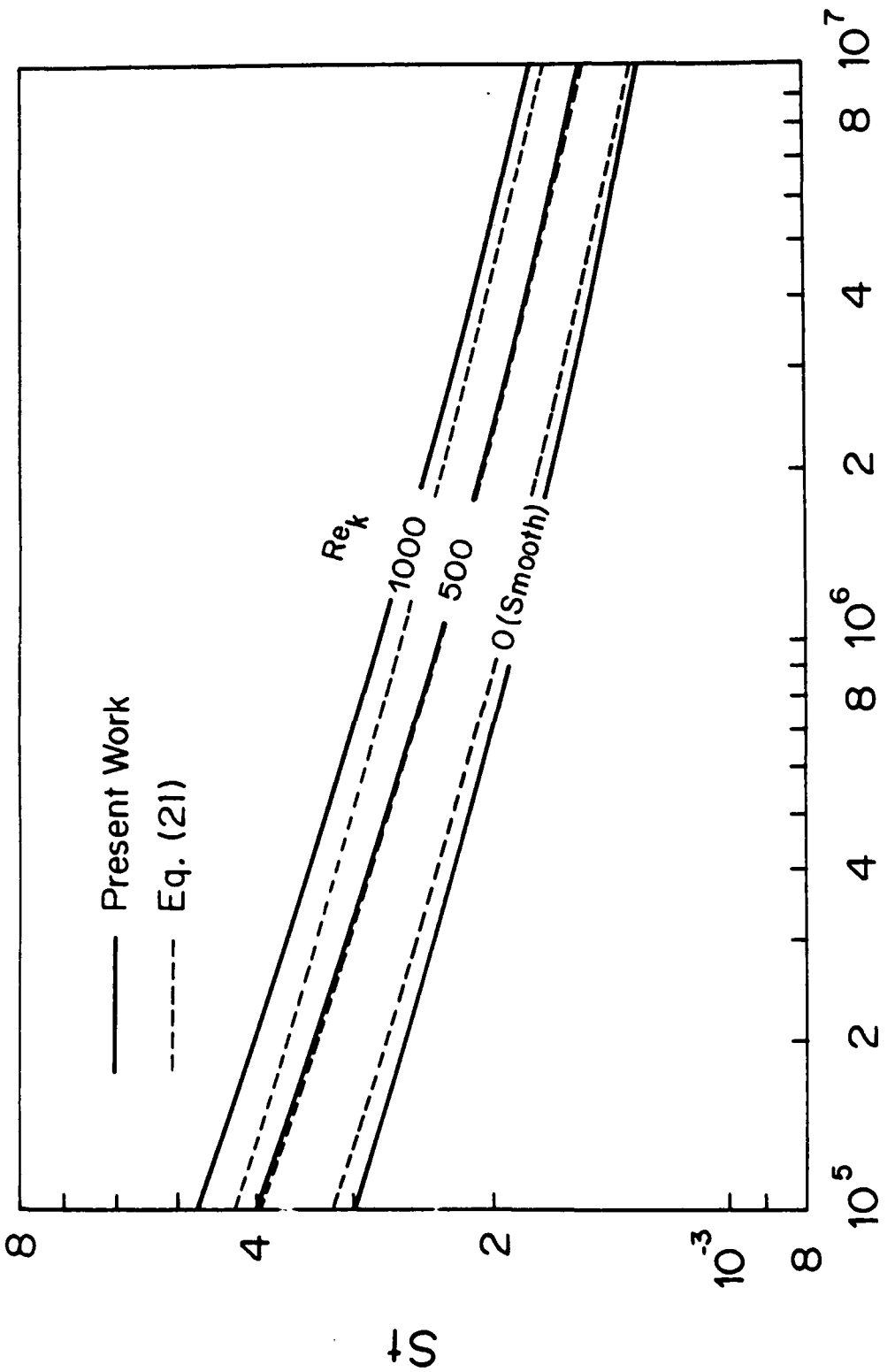

Figure 30. Comparison With Dippery and Sabersky's Similarity Law.

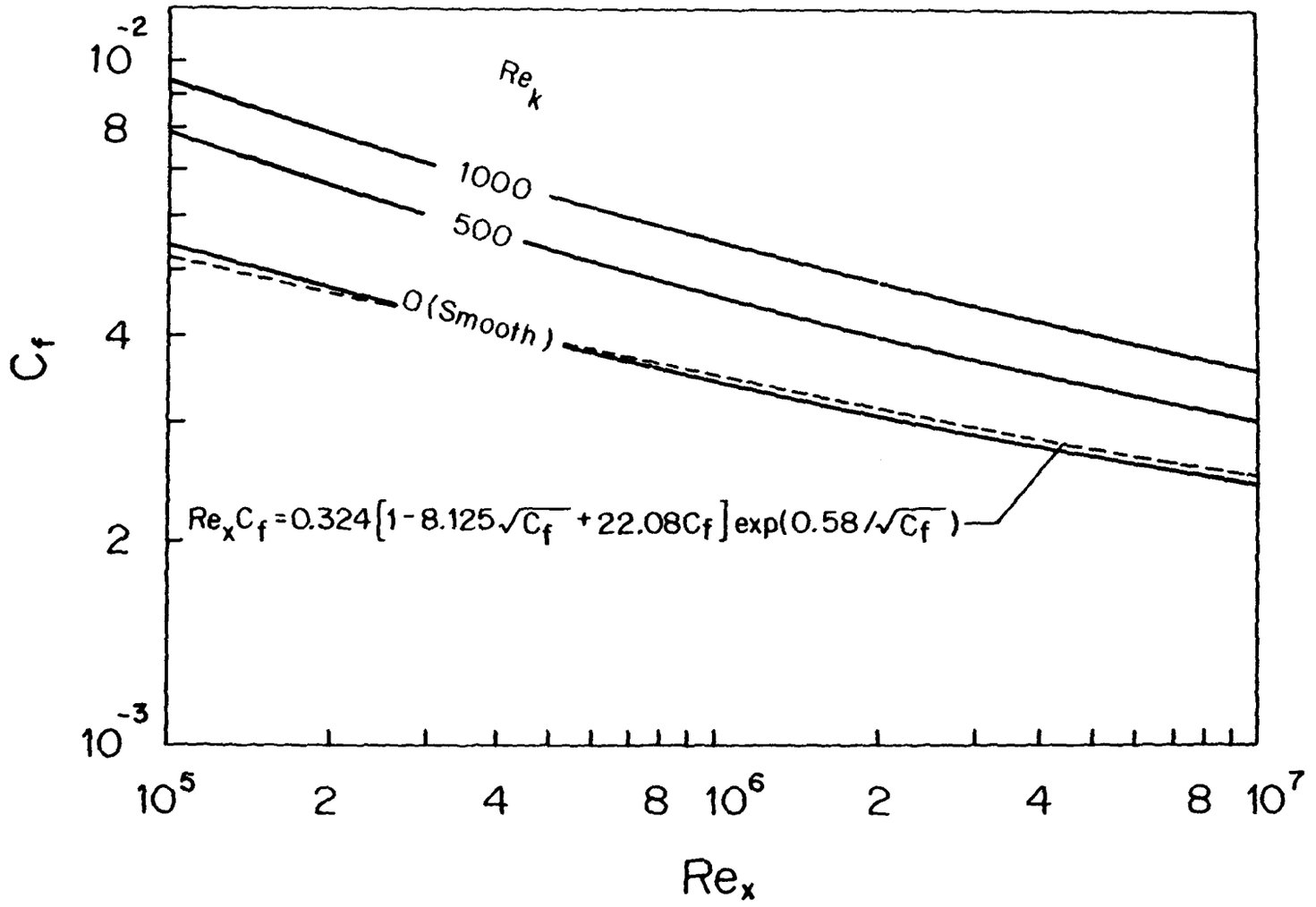

Figure 31. Friction Coefficients for Re_k = O (Smooth), 500, 1000

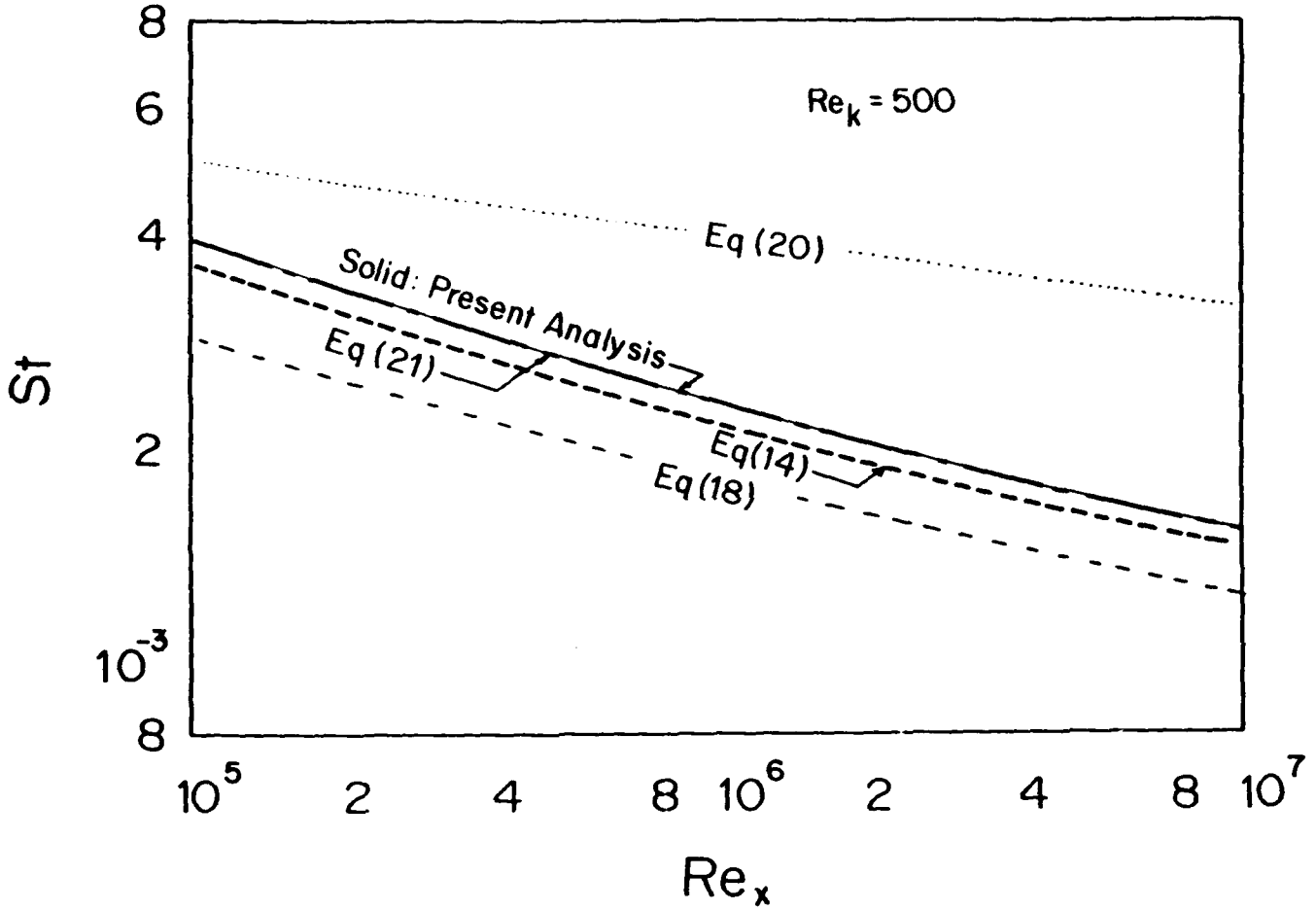

Figure 32. Stanton Number Comparison With Correlation Equations.

V. CONCLUSIONS AND RECOMMENDATIONS

Essentially retaining the concept of Prandtl's mixing length theory, an earlier research has successfully expressed the rough-wall mixing length by an exponential form in terms of a local velocity in treating flows over rough surfaces. Extending this approach to thermal boundary layer analysis, a thermal mixing length is similarly postulated so that experimental attributes in thermal layers are properly modeled, especially the downshift of the temperature from the thermal wall-law. The models thus formed are shown to predict heat transfer in good accord with the similarity law of Dippery and Sabersky [7], based on their experimental data in rough-wall pipe flows. The new formulations in the present work have the same constraints as does the mixing length for smooth surfaces by Cebeci [3] in that the extension to flows with pressure gradients needs special treatments.

Previous investigations by McDonald [17] and by Perry and Joubert [20] have shown that for flows with moderate pressure gradients, the velocity shift concept is still valid. It appears reasonable to assume that this applies equally to thermal boundary layers, pending further research for substantiation. Extensions into other parametric variations are, naturally, to be studied to enlarge its range of applications. The operating parameters are pressure gradient, mass transfer, compressibility, and limiting eddy conductivity at the outer edge of the boundary layer. In addition, the effect of surface roughness variation in the streamwise direction and nonisothermal surface are needed to render the model more useful.

REFERENCES

1. Bammert, K., and Woelk, G.U., "The Influence of the Blading Surface Roughness on the Aerodynamic Behavior and Characteristic of an Axial Compressor," J. Eng'g for Power, v. 102, pp. 283-287, April 1980.

2. Barnerian, G., and NcKillop, A.A., "The Effect of Surface Roughness in Nozzle Heat Transfer," Paper No. FC6.2, International Heat Transfer Conference, Tokyo, Vol. 2, pp. 234-238, 1974.

3. Cebeci, T., "A Model for Eddy Conductivity and Turbulent Prandtl Number," J Heat Transfer, pp. 227-234, May 1973.

4. Chevray, R., and Kovasznay, L.S.G., "Turbulence Measurements in the Wake of a Thin Flat Plate," AIAA J., v. 7, no. 8, pp. 1641-1643, Aug. 1969.

5. Christoph, G.H., and Pletcher, R.H., "Prediction of Rough Wall Skin Friction and Heat Transfer," AIAA Paper No. 82-0031, Orlando, Fla., 1982.

6. Coleman, H.W., Hodge, B.K., and Taylor, R.P., "A Reevaluation of Schlichting's Surface Roughness Experiment," J Fluids Eng'g., v. 106, pp. 60-85, Mar 1984.

7. Dippery, D.F., and Sabersky, R.H., "Heat and Mass Transfer in Smooth and Rough Tubes at Various Prandtl Numbers," Int. J. Heat and Mass Transfer, vol. 6, pp. 329-353, 1963.

8. Dirling, R.B., "A Method of Computing Roughwall Heat Transfer," AIAA Paper No. 73-763, The 8th Thermophysics Conference, July 1973.

9. Dvorak, F.A., "Calculation of Turbulent Boundary Layers on Rough Surfaces," AIAA J., v. 7, no. 9, pp. 1752-1759, Sept. 1969.

10. Finston, M.L., "A Model for Rough Wall Turbulent Heating and Skin Friction," AIAA Paper No. 82-0199, The 20th AeroSpace Science Meeting, Jan. 1982.

11. Hama, F.R., "Boundary Layer Characteristics for Smooth and Rough Surfaces," Trans. Soc. Naval Arch. & Marine Engrs., v. 62, pp. 333-355, 1954.

12. Han, L.S., Turbulent Flow over Rough Turbine Airfoils, AFWAL-TR-85-2056, Aug 1985, Final Contract Report, The Ohio State University.

13. Kadar, B.A., Yaglom, A.M., "Heat and Mass Transfer Laws for Fully Turbulent Wall Flows," Int. J. Heat Mass Transfer, vol. 15, pp. 2329-2351, 1972.

14. Kays, W.M., and Crawford, M.E., Convective Heat and Mass Transfer, McGraw-Hill Book Co., 1980.

15. Ligrani, P.M., and Moffat, R.J., "Structure of Transitionally Rough and Fully Rough Turbulent Boundary Layers," J. Fluid Mech., vol. 162, pp. 69-98, 1986.

16. Moffat, R.J., Heazler, J.M., and Kays, W.M., "Experimental Heat Transfer Behavior of a Turbulent Boundary Layer on a Rough Surface with Blowing," J. Heat Transfer, vol. 100, pp. 134-142, Feb. 1976.

17. McDonald, H., "The Effect of Pressure Gradient on the Law of the Wall in Turbulent Flow," J. Fluid Mech., vol. 35, part 2, pp. 311-366, 1969.

18. Na, T.Y., and Habib, I.S., "Heat Transfer in Turbulent Pipe Flow Based on a New Mixing Length Model," App. Sci. Res., vol. 28, pp. 302-314, Nov. 1973.

19. Norris, R.H., "Some Simple Approximate Heat Transfer Correlation for Turbulent Flow in Ducts with Rough Surfaces," Augmentation of Heat and Mass Transfer, ASME Publication, Winter Annual Meetings, 1970.

20. Perry, A.E., Joubert, P.N., "Rough-Wall Boundary Layers in Adverse Pressure Gradients," J. Fluid Mech., vol. 17, pp. 193-211, 1963.

21. Schlichting, H., Boundary Layer Theory, McGraw-Hill Book Co., 1968.

22. Spading, D.B., and Chi, S.W., "The Drag of a Compressible Turbulent Boundary Layer on a Smooth Flat Plate with and without Heat Transfer," J. Fluid Mech., vol. 18, pp. 117-143, 1964.

23. Simpson, R.L., et al., "An Experimental Study of the Turbulent Prandtl Number of Air with Injection and Suction," Int J Heat Mass Transfer, vol. 13, pp. 125-141, 1970.

24. Tani, I., Hama, R., and Mituisi, S., "On the Permissible Roughness in the Laminar Boundary Layer," Technical Report, Aero. Res. Inst., Tokyo, 1940.

25. van Driest, E.R., "On Turbulent Flow Near a Wall," J. Aeronautical Sci., vol. 23, pp. 1007-1011, 1956.

26. Vilemas, J.V., and Adomaitis, J.E.J, "Heat Transfer and Friction of a Rough Cylinder in Longitudinal Turbulent Gas Flow," Int J Heat Mass Transfer, vol. 31, no. 8, pp. 1669-1677, 1988.

27. Voisinet, R.L., Influence of Roughness and Blowing on Compressible Boundary Layer Flow, Naval Surface Weapons Center, Report No. NSWC TR-79-153.

* U.S.Government Printing Office 1990-748-056/24302